3-29-2004

Benefit of Staged Cooling In Shrink Fitted Composite Cylinders

Nathaniel Oren Collier
University of South Florida

Benefit of Staged Cooling

In Shrink Fitted Composite Cylinders

by

Nathaniel Oren Collier

A thesis submitted in partial fulfillment
of the requirements for the degree of
Master of Science in Mechanical Engineering
Department of Mechanical Engineering
College of Engineering
University of South Florida

Major Professor: Autar K. Kaw, Ph.D.
Glen H. Besterfield, Ph.D.
Muhammad M. Rahman, Ph.D.

Date of Approval:
March 29, 2004

Keywords: bascule bridge, transient, thermal stress, nonhomogeneous material properties

TABLE OF CONTENTS

LIST OF TABLES ii

LIST OF FIGURES iii

ABSTRACT v

CHAPTER 1 – INTRODUCTION 1

Literature Survey 2

Current Study 4

CHAPTER 2 – PROBLEM FORMULATION 6

Thermal Formulation 7

Thermal Boundary Conditions 10

Elasticity Formulation 11

Elasticity Boundary Conditions 20

Failure Criteria 23

CHAPTER 3 – RESULTS 26

Conclusions 33

REFERENCES 35

APPENDICES 37

Appendix 1: Property Data for Cylinder Material 38

Appendix 2: Convection Medium Property Data 43

Appendix 3: Program Flow 49

Appendix 4: Verification 50

Appendix 5: Convergence Test 52

Appendix 6: Tables of Results 54

LIST OF TABLES

Table 1.	Geometric Data for the Three Bridges	26
Table 2.	Constants C_{FN2} Used in Finding Cylinder Tolerances	27
Table A1.	Elastic Properties of Steel as a Function of Temperature	38
Table A2.	Thermal Properties of Steel as a Function of Temperature	40
Table A3.	Fracture Toughness of ASTM E-24 Steel as a Function of Temperature	42
Table A4.	Convection Coefficient for Liquid Nitrogen as a Function of Temperature	44
Table A5.	Property Data for Air as a Function of Temperature	46
Table A6.	Property Data for Isopropyl Alcohol as a Function of Temperature	46
Table A7.	Results for the Christa McAuliffe in Cooling Process 1	54
Table A8.	Results for the Christa McAuliffe in Cooling Process 2	55
Table A9.	Results for the Christa McAuliffe in Cooling Process 3	56
Table A10.	Results for Hillsborough Ave. in Cooling Process 1	57
Table A11.	Results for Hillsborough Ave. in Cooling Process 2	58
Table A12.	Results for Hillsborough Ave. in Cooling Process 3	59
Table A13.	Results for 17th St. Causeway in Cooling Process 1	60
Table A14.	Results for 17th St. Causeway in Cooling Process 2	61
Table A15.	Results for 17th St. Causeway in Cooling Process 3	62

LIST OF FIGURES

Figure 1.	A Bascule Bridge	1
Figure 2.	Completely Assembled Trunnion-Hub-Girder (THG) System	2
Figure 3.	THG Assembly Procedures	3
Figure 4.	Geometry of the Composite Cylinder	6
Figure 5.	Thermal Conductivity and Specific Heat for Cylinder Material as a Function of Temperature	8
Figure 6.	Nodal Locations along Cylinder Wall	9
Figure 7.	Coefficient of Thermal Expansion as a Function of Temperature	18
Figure 8.	Fracture Toughness and Yield Strength as a Function of Temperature	25
Figure 9.	Geometry of Trunnion-Hub Assembly	26
Figure 10.	Overall Minimum Critical Crack Length as a Function of Hub-Trunnion Thickness Ratio for the Christa McAuliffe Bridge	29
Figure 11.	Overall Minimum Stress Ratio as a Function of Hub-Trunnion Thickness Ratio for the Christa McAuliffe Bridge	29
Figure 12.	Overall Minimum Critical Crack Length as a Function of Hub-Trunnion Thickness Ratio for the Hillsborough Ave. Bridge	31
Figure 13.	Overall Minimum Stress Ratio as a Function of Hub-Trunnion Thickness Ratio for the Hillsborough Ave. Bridge	31
Figure 14.	Overall Minimum Critical Crack Length as a Function of Hub-Trunnion Thickness Ratio for the 17th St. Causeway Bridge	32
Figure 15.	Overall Minimum Stress Ratio as a Function of Hub-Trunnion Thickness Ratio for the 17th St. Causeway Bridge	32

Figure A1.	Young's Modulus of ASTM A203-A Steel as a Function of Temperature	39
Figure A2.	Poisson's Ratio of ASTM A203-A Steel as a Function of Temperature	39
Figure A3.	Tensile Strength of ASTM A203-A Steel as a Function of Temperature	39
Figure A4.	Yield Strength of ASTM A203-A Steel as a Function of Temperature	39
Figure A5.	Thermal Conductivity of ASTM A203-A Steel as a Function of Temperature	40
Figure A6.	Specific Heat of ASTM A203-A Steel as a Function of Temperature	40
Figure A7.	Density of ASTM A203-A Steel as a Function of Temperature	41
Figure A8.	Coefficient of Thermal Expansion of ASTM A203-A Steel as a Function of Temperature	41
Figure A9.	Fracture Toughness and Yield Strength as a Function of Temperature	41
Figure A10.	Heat Flux Versus Temperature Difference for Liquid Nitrogen	43
Figure A11.	Convection Coefficient for Liquid Nitrogen as a Function of Wall Temperature	45
Figure A12.	Convection Coefficient for Air as a Function of Wall Temperature for a Diameter = 1 in	48
Figure A13.	Convection Coefficient for Dry-Ice/Alcohol as a Function of Wall Temperature for a Diameter = 1 in	48
Figure A14.	Flow Chart of Computer Program	49
Figure A15.	Comparison of Exact and Programmed Solution to the Water Problem	50
Figure A16.	Comparison of Exact and Programmed Solution to the Air Problem	51

BENEFIT OF STAGED COOLING
IN SHRINK FITTED COMPOSITE CYLINDERS

Nathaniel Collier

ABSTRACT

To assemble the fulcrum of bascule bridges, a trunnion is immersed into liquid nitrogen so that it can be shrunk fit into the hub. This is followed by immersing the resulting trunnion-hub assembly into liquid nitrogen so that it can be then shrunk fit into the girder. On one occasion in Florida, when the trunnion-hub assembly was put into liquid nitrogen, development of cracks on the hub was observed. Experimental and numerical studies conducted since 1998 at University of South Florida show that the cracking took place due to combination of high interference stresses in the trunnion-hub assembly, low fracture toughness of steel at cryogenic temperatures, and steep temperature gradients due to sudden cooling.

In this study, we are studying the benefit of staged cooling to avoid cracking in the trunnion-hub assembly when it is cooled down for shrink fitting. We looked at three cooling processes - 1) Direct immersion into liquid nitrogen 2) Immersion into a refrigerated chamber, then liquid nitrogen 3) Immersion into a refrigerated chamber, then a dry-ice/alcohol bath, and finally liquid nitrogen.

The geometry of the trunnion-hub assembly was approximated by a composite made of two infinitely long hollows cylinders. The transient problem of temperature distribution and the resulting stresses was solved using finite difference method. Using critical crack lengths and Von-Mises stress as failure criteria, the three cooling processes were compared.

The study showed that the minimum critical crack length and stress ratio is increased by as much as 200% when cooling first in refrigerated air followed by liquid nitrogen. However, there is little benefit from adding dry-ice/alcohol as an intermediate step in the cooling process.

CHAPTER 1 – INTRODUCTION

Although the analysis of composite cylinders has many applications in various disciplines, this particular analysis was done as part of a specific study at the University of South Florida on the subject of bascule bridges. A bascule bridge is what is more commonly known as a draw bridge. The draw bridges of the medieval times were designed to keep invaders out of a castle. The draw bridges of today are used to allow water traffic to pass underneath roadways. Although the use of these bridges is different, the basic concept is the same. They work like a lever that rotates around a central point known as the fulcrum. Depicted in Fig. 1, the lever is the roadway and the fulcrum is a trunnion.

Figure 1. A Bascule Bridge

The critical point of this kind of bridge design is the fulcrum. The fulcrum is inserted into the bridge girder. When the bridge is raised, the motors apply torque to the fulcrum which rotates the bridge. This means that the fulcrum must be securely fastened to the bridge. For this reason, a trunnion is used and is supported by a hub, which is inserted to the bridge as well as bolted to the girder. This assembly is referred to as the trunnion-hub-girder (THG) system and is seen constructed in Figure 2. Due to the need for strength, an interference fit such as FN2 and FN3 (Shigley, 1986) is used to construct the THG assembly. Currently, two procedures are followed in the United States of America to make the THG assembly.

- AP#1: The trunnion is shrunk in liquid nitrogen (or some cold fluid, cold enough to provide enough shrinkage) and inserted into the hub. The same step is then repeated on the resulting trunnion-hub assembly for insertion into the girder.

- AP#2: In this procedure, the hub is first shrink fitted into the girder. This is then followed by the trunnion being shrink fitted into hub-girder assembly.

It is this shrink fitting process that is the subject of much study. As a material gets colder, it becomes more likely to crack. There have been problems encountered during this THG assembly. According to the Florida Department of Transportation (FDOT), the first method of construction produced cracks in the THG assembling process for the Christa McAuliffe Bridge. The failure of this assembly is expensive to replace and delays the bridge construction. For this reason, a study is being conducted to determine why the THG assemblies failed during assembly and how the problem can be avoided in the future.

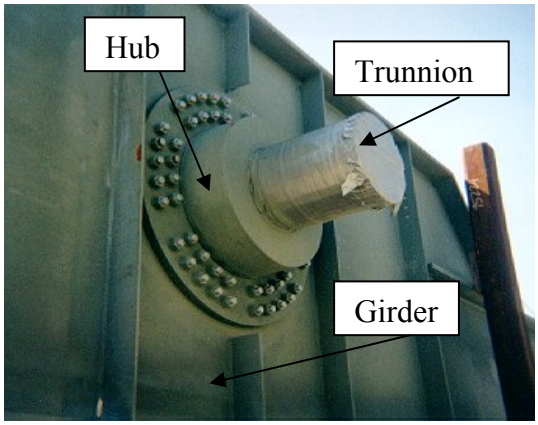

Figure 2. Completely Assembled Trunnion-Hub-Girder (THG) System

Literature Survey

Although the topic of composite cylinders has a much broader scope than that mentioned here, there are several individual studies conducted on this specific problem—that of the cracking of the THG assembly during assembly. The following describes their contribution.

To aid in the design of these bridges, Denninger (2000) developed a series of design tools, which calculated the torque needed to lift the bridge, found the stresses in the THG assembly, and developed a bolt pattern used to supplement the hub-girder fit. Although his work was mainly to develop tools for study of these bridges, Denninger concluded that the steady state stresses were well below the ultimate tensile strength of the material. Thus, it was determined that the cause of failure must come from the transient stresses of the assembly process.

Figure 3. THG Assembly Procedures

Ratnam (2000) conducted a finite element analysis on the two THG assembly procedures shown in Fig. 3. He used this model to analyze the stresses, temperatures and critical crack lengths for both procedures. His study concluded that assembly procedure AP#2 resolves the problems encountered with the AP#1. However, Ratnam also suggested that there could be a THG geometry where assembly procedure AP#1 is safer than AP#2. For this reason, each THG assembly must be analyzed by a method detailed in his study (Ratnam, 2000) to determine which procedure is preferred.

Nichani (2001) experimentally studied the two currently used assembly procedures. The experiment was conducted with thermocouples and strain gauges at critical points in the design. The complete procedure was logged and the stresses calculated from the measured strains. These stresses were compared with the yield

strength, and the critical crack length. The results of this experiment agree with Ratnam's conclusions—that there is a favorable method of assembly with respect to yield stress and critical crack length. Assembly procedure AP#2 was safer based on the stated criteria.

Current Study

The studies conducted by Ratnam (2000) and Nichani (2001) focused on alternative methods of assembly due to the fact that assembly method one had produced failure in the past. They both concluded that assembly procedure AP#2 was preferred to AP#1. The problem with implementing AP#2, is that in many cases the trunnion-hub assembly is manufactured elsewhere and then sent to the job site for insertion. Assembly procedure AP#2 would require that the complete trunnion-hub-girder assembly is done on the job site.

For this reason, the goal of this study is to return to assembly procedure AP#1 and determine if staged cooling can alleviate the encountered problems. In the Christa McAuliffe Bridge, the trunnion-hub (TH) cracked while being cooled for insertion in to the girder. Therefore, only the step of assembly where the trunnion-hub is cooled will be studied.

The current method of cooling uses liquid nitrogen, which boils at -321°F. This severe thermal gradient causes the material to cool very quickly, inducing high thermal stresses. Cooling in stages by use of a refrigerated chamber at -30°F and a dry-ice/alcohol bath at -108°F would certainly be of benefit to the integrity of the THG assembly process. This method, however, is also sure to cost more money and time. This study hypothesizes that staged cooling will significantly increase the overall minimum critical crack length, making the assembly procedure safer.

Therefore, a numerical analysis was conducted, simulating the trunnion-hub assembly in different stages of cooling. This is to represent the portion of the THG assembly process where the trunnion-hub assembly is cooled for insertion into the girder. Three different cooling processes were studied.

- Process 1 - Direct immersion into liquid nitrogen

- Process 2 - Immersion into a refrigerated chamber, then liquid nitrogen
- Process 3 - Immersion into a refrigerated chamber, then a dry-ice/alcohol bath, and finally liquid nitrogen

The analysis was conducted by the method of finite differences to solve the governing differential equations.

For simplicity, the trunnion-hub assembly was modeled as a composite cylinder. This assumption is valid to make since the goal is not to develop specific numbers, but to quantify the benefit of one procedure over another. It is assumed that the trunnion-hub assembly will behave similarly to a composite cylinder. This problem is not a complicated one to solve under the normal assumption of constant material properties. However, due to the wide range of temperatures, the materials properties need to be assumed as functions of temperature.

CHAPTER 2 – PROBLEM FORMULATION

The geometry of a trunnion-hub assembly was simplified as a composite cylinder. This simplification was made so that the finite differencing would be a feasible method of solving for all unknowns. It should also be noted that the exact stresses and critical crack ratios are not of interest here. The purpose is to compare cooling methods. This fact justifies for many such simplifications to be made. The more important question is relatively quantifying how much staged cooling benefits the TH assembly process. Figure 4 shows these cylinders as well as explains some of the notation to be used.

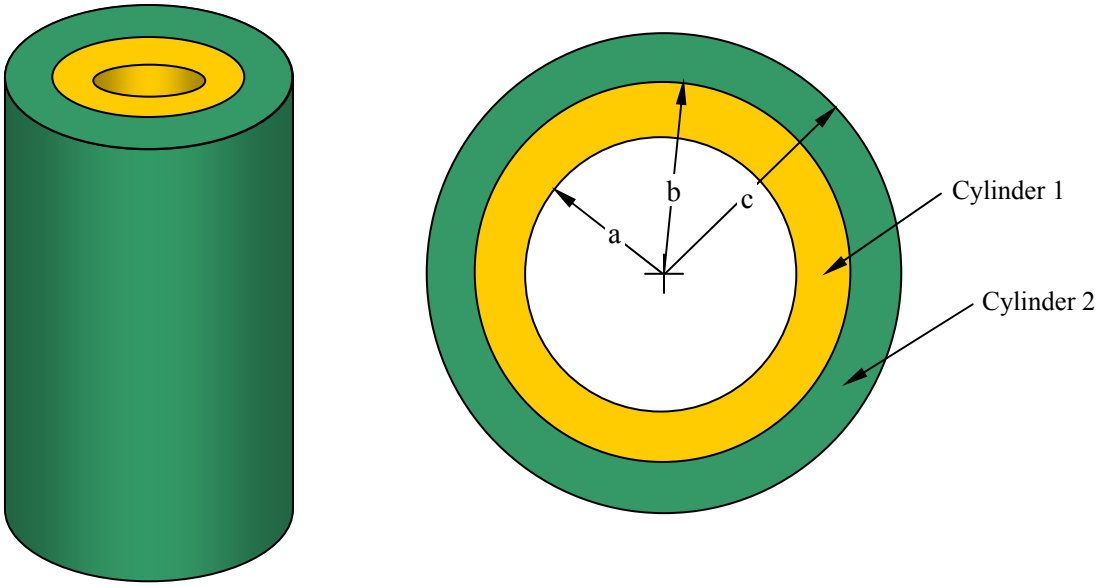

Figure 4. Geometry of the Composite Cylinder

Thermal Formulation

To determine the effect of thermal stresses, it is first necessary to know the temperature distribution within the cylinders as a function of space and time. The composite cylinder is to be immersed in several media and will be cooled solely by convection. This problem is axisymmetric and solved in a cylindrical coordinate system. Each cylinder is treated as a separate cylinder, linked by boundary conditions.

The governing equation for each cylinder is as follows:

$$\rho_j(T)C_{p_j}(T)\frac{\partial T_j}{\partial t} = \frac{1}{r}\frac{\partial}{\partial r}\left[r \cdot k_j(T)\frac{\partial T_j}{\partial r}\right] \tag{1}$$

where,

$T = f(r,t)$ and is the temperature distribution,

subscript $j = 1, \text{and } 2$ and designates Cylinders 1 and 2, respectively,

ρ is the material density,

C_p is the material specific heat,

k is the material thermal conductivity,

T is the radial temperature distribution,

r is radial position, and

t is time.

Equation (1) (Özişik, 1993) is used to govern both cylinders but is applied separately so that the cylinders can differ in material properties. Since the cylinders will be subjected to cryogenic temperatures it is necessary to assume that all material properties are functions of temperature. Note the variance of thermal conductivity and specific heat over temperature in Fig. 5. The thermal conductivity doubles over the range of temperature of interest. The specific heat at room temperature is six times greater than that at the ambient temperature of liquid nitrogen. Thus the normal simplification of assuming constant material properties is not valid for Eq. (1).

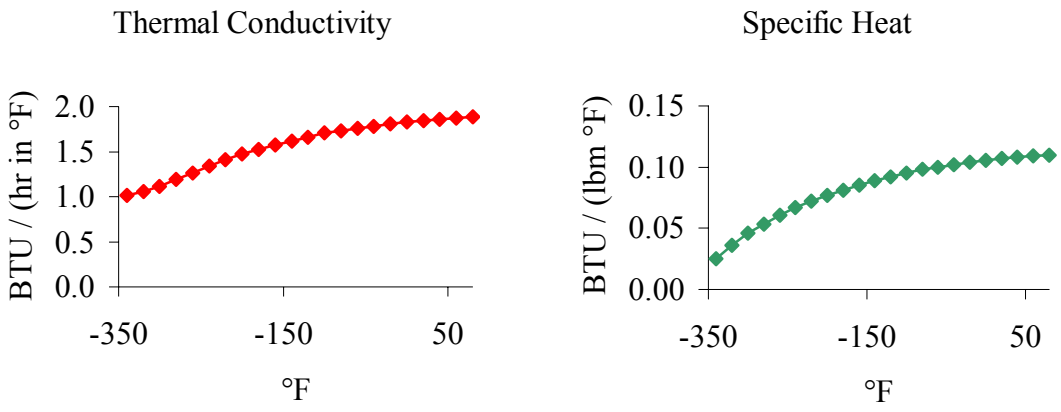

Figure 5. Thermal Conductivity and Specific Heat for Cylinder Material as a Function of Temperature

This analysis used finite differencing for the solution of differential equations. Finite differencing replaces derivatives with approximations using discrete points. A computer program was written to perform the necessary calculations rapidly. Because computers are never exact in their calculations, errors always exist. In transient problems, the radial temperature distribution is found at each time step and is usually based in part on the previous time step. This causes the small errors in calculations to propagate as further time steps are calculated resulting in a phenomenon called instability. Most methods of solving transient problems have a stability criterion which limits either the number of nodes or the time step in the solution. This is not desirable because a designer wishes to have complete control over the simulation and for the simulation to always be stable. The Crank-Nicolson method is used in this simulation because it is unconditionally stable. (Özişik, 1993).

$$\left(\rho_j \cdot C_{p_j}\right)_i \frac{T_{j,i}^{n+1} - T_{j,i}^{n}}{\Delta t} = \frac{1}{2}\frac{1}{r_i}\frac{1}{\Delta r_j^{\,2}}\left[\left(k_j \cdot r\right)_{i+\frac{1}{2}}\left(T_{j,i+1}^{n+1} - T_{j,i}^{n+1}\right) - \left(k_j \cdot r\right)_{i-\frac{1}{2}}\left(T_{j,i-1}^{n+1} - T_{j,i}^{n+1}\right)\right] + \frac{1}{2}\frac{1}{r_i}\frac{1}{\Delta r_j^{\,2}}\left[\left(k_j \cdot r\right)_{i+\frac{1}{2}}\left(T_{j,i+1}^{n} - T_{j,i}^{n}\right) - \left(k_j \cdot r\right)_{i-\frac{1}{2}}\left(T_{j,i-1}^{n} - T_{j,i}^{n}\right)\right] \quad (2)$$

where,

subscript i designates a nodal location, and

superscript n designates a time step.

The properties at each node are evaluated at the temperature of the previous time step. This is incorrect but insignificant if the time step is small enough. This method is unconditionally stable and second order accurate. The cylinder was discretized as shown below in Fig. 6 and this equation was used for all interior nodes (nodes 1 to *N*-1 of Cylinder 1 and nodes 1 to *M*-1 of Cylinder 2). N represents the number of nodes in Cylinder 1, and M represents the number of nodes in Cylinder 2. The boundary nodes are discussed below.

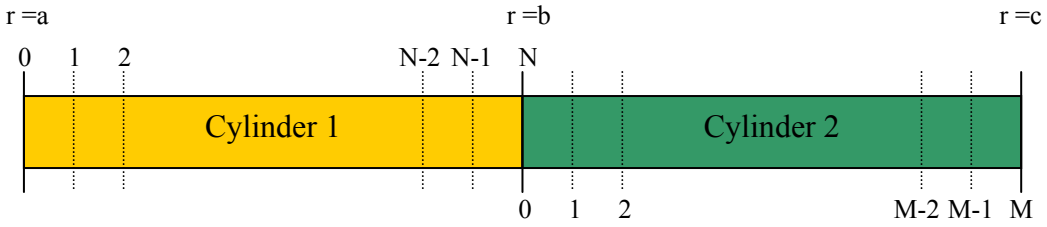

Figure 6. Nodal Locations along Cylinder Wall

This generates a system of linear equations, which are solved using matrix algebra to determine the nodal temperatures. Before this can happen, the boundary conditions must be applied to the problem.

Thermal Boundary Conditions

In each case the cylinder is rapidly cooled by various media. Cylinder 1 is experiencing convection on its inner surface. Therefore the boundary condition on the inner edge at $r = a$ is:

$$-k_1(T)\frac{\partial T_1}{\partial r} = h(T)\cdot\left(T_1(r,t)\big|_{r=a} - T_{amb}\right) \tag{3}$$

where,

h is the convection coefficient of the cooling medium, and

T_{amb} is the ambient temperature of the cooling medium.

A second order accurate forward divided difference approximation (Boresi, 1991) is used for the derivative term. The thermal conductivity is evaluated at the wall temperature and the convection coefficient is evaluated at the average of the wall and ambient temperature.

$$-k_1(T_{1_0}^n)\left[\frac{1}{2\cdot\Delta r_1}\left(-3\cdot T_{1_0}^{n+1} + 4\cdot T_{1_1}^{n+1} - T_{1_2}^{n+1}\right)\right] = h(\frac{T_{1_0}^n + T_{amb}}{2})\left(T_{1_0}^{n+1} - T_{amb}\right) \tag{4}$$

Similarly, Cylinder 2 is also experiencing convection on its outer surface at $r = c$. A second order accurate backward divided difference approximation is used for this derivative term.

$$-k_2(T)\frac{\partial T_2}{\partial r} = h(T)\cdot\left(T_2(r,t)\big|_{r=c} - T_{amb}\right) \tag{5}$$

$$-k_2(T_{2_M}^n)\left[\frac{1}{2\cdot\Delta r_2}\left(3\cdot T_{2_M}^{n+1} - 4\cdot T_{2_{M-1}}^{n+1} + T_{2_{M-2}}^{n+1}\right)\right] = h(\frac{T_{2_M}^n + T_{amb}}{2})\left(T_{2_M}^{n+1} - T_{amb}\right) \tag{6}$$

The two interface conditions are due to the fact that the temperature and the heat flux must be equal at the interface, $r = b$. This means that,

$$T_1(r,t)\big|_{r=b} = T_2(r,t)\big|_{r=b} \tag{7}$$

$$T_{1_N}^{n+1} = T_{2_0}^{n+1} \tag{8}$$

and,

$$-k_1(T)\frac{\partial T_1}{\partial r} = -k_2(T)\frac{\partial T_2}{\partial r} \tag{9}$$

In this case a backward difference approximation must be used for the derivative of T_1 and a forward difference approximation for T_2.

$$\begin{aligned} &-k_1(T_{1_0}^n)\left[\frac{1}{2\cdot\Delta r_1}\left(3\cdot T_{1_N}^{n+1}-4\cdot T_{1_{N-1}}^{n+1}+T_{1_{N-2}}^{n+1}\right)\right] \\ &=-k_2(T_{2_M}^n)\left[\frac{1}{2\cdot\Delta r_2}\left(-3\cdot T_{2_0}^{n+1}+4\cdot T_{2_1}^{n+1}-T_{2_2}^{n+1}\right)\right] \end{aligned} \tag{10}$$

These interface conditions, Eqs. (8,10), link the differential equation of each cylinder.

Thus the governing equation is used for interior nodes and the boundary condition equations are used for the boundary nodes. What results is a system of linear equations where the unknowns are the nodal temperatures (at time step, $n+1$). This system of linear equations is solved progressively for each time step. The nodal temperatures obtained for one time step are used to calculate the nodal temperatures for the next time step.

Elasticity Formulation

Once the temperature distribution at a particular time step is known, the thermal stresses can be calculated. The composite cylinder experiences stress from two sources: thermal gradient and the pre-imposed interface fit. The inner cylinder is actually too large to be placed in the outer cylinder. It is shrunk in a cold medium and inserted into the outer cylinder. In this study, this process is already assumed to have taken place. What results is a pressure at the interface that becomes a source of stress in the composite cylinder.

For this portion of the simulation, equilibrium must be satisfied. When formulating a problem, it is sometimes difficult to choose the form in which one wants the equations. Many times the boundary conditions can help make that decision. In this case, it is desirable to have the equations only in terms of displacements. All other desired quantities are calculated directly from displacements. The following are the three equations of equilibrium (Timoshenko, 1951):

$$\frac{\partial\sigma_{rj}}{\partial r}+\frac{1}{r}\frac{\partial\tau_{r\theta j}}{\partial\theta}+\frac{\sigma_{rj}-\sigma_{\theta j}}{r}+\frac{\partial\tau_{rzj}}{\partial z}=0 \tag{11}$$

$$\frac{1}{r}\frac{\partial \sigma_{\theta j}}{\partial \theta}+\frac{\partial \tau_{r\theta j}}{\partial r}+\frac{\partial \tau_{\theta z j}}{\partial z}+\frac{2\tau_{r\theta j}}{r}=0 \tag{12}$$

$$\frac{\partial \sigma_{z j}}{\partial z}+\frac{\partial \tau_{zr j}}{\partial r}+\frac{1}{r}\frac{\partial \tau_{\theta z j}}{\partial \theta}+\frac{1}{r}\tau_{rz j}=0 \tag{13}$$

where,

σ_r is the radial stress,

σ_θ is the hoop stress,

σ_z is the longitudinal stress, and

$\tau_{r\theta}$, τ_{rz}, and $\tau_{\theta z}$ are the shear stresses in the *rθ*, *rz*, and *θz* planes, respectively.

Equations (11-13) are all in terms of stress. To get them into displacements as desired they must be first related to strains. The following are the stress-strain equations. They have been modified to account for thermal stresses (Timoshenko, 1951).

$$\varepsilon_{r j}-\phi_j(T)=\frac{1}{E_j(T)}\left[\sigma_{r j}-\upsilon_j(T)\left(\sigma_{\theta j}+\sigma_{z j}\right)\right] \tag{14}$$

$$\varepsilon_{\theta j}-\phi_j(T)=\frac{1}{E_j(T)}\left[\sigma_{\theta j}-\upsilon_j(T)\left(\sigma_{r j}+\sigma_{z j}\right)\right] \tag{15}$$

$$\varepsilon_{z j}-\phi_j(T)=\frac{1}{E_j(T)}\left[\sigma_{z j}-\upsilon_j(T)\left(\sigma_{\theta j}+\sigma_{r j}\right)\right] \tag{16}$$

$$\gamma_{r\theta j}=\frac{\tau_{r\theta j}}{G_j(T)} \tag{17}$$

$$\gamma_{\theta z j}=\frac{\tau_{\theta z j}}{G_j(T)} \tag{18}$$

$$\gamma_{rz j}=\frac{\tau_{rz j}}{G_j(T)} \tag{19}$$

where,

$$\phi_j(T)=\int_{T_{initial}}^{T_j(r)}\alpha_j(T')dT' \tag{20}$$

ε_r is radial strain,

ε_θ is strain in the hoop strain,

ε_z is longitudinal strain,

$\gamma_{r\theta}$, $\gamma_{\theta z}$, and γ_{rz} are shear strains in the *rθ*, *θz*, and *rz* planes, respectively,

α is the coefficient of thermal expansion,

E is the modulus of elasticity,

G is the modulus of rigidity, and

υ is Poison's ratio.

Then the strains are, by definition, expressed as follows (Timoshenko, 1951):

$$\varepsilon_{rj} = \frac{\partial u_{rj}}{\partial r} \tag{21}$$

$$\varepsilon_{\theta j} = \frac{1}{r}\frac{\partial u_{\theta j}}{\partial r} + \frac{u_{rj}}{r} \tag{22}$$

$$\varepsilon_{zj} = \frac{\partial u_{zj}}{\partial z} \tag{23}$$

$$\gamma_{r\theta j} = \frac{1}{r}\frac{\partial u_{rj}}{\partial \theta} + \frac{\partial u_{\theta j}}{\partial r} - \frac{u_{\theta j}}{r} \tag{24}$$

$$\gamma_{rzj} = \frac{\partial u_{rj}}{\partial z} + \frac{\partial u_{zj}}{\partial r} \tag{25}$$

$$\gamma_{\theta zj} = \frac{\partial u_{\theta j}}{\partial z} + \frac{1}{r}\frac{\partial u_{zj}}{\partial \theta} \tag{26}$$

where,

u_r is the radial displacement,

u_θ is the angular displacement, and

u_z is the longitudinal displacement.

Solving these fifteen equations (Eqs. 11-26) can be intractable, but there are several simplifications that can be made in this study. The problem is axisymmetric. This means that at any constant radial location from the center, the displacements, stresses, and strains will be the same. There will be no displacement in the θ-direction either. Therefore, all equations which contain u_θ or any derivative of θ are eliminated. The equations then look more manageable. Notice that Eqs. (27), (28), and (34) have become simplified as well.

$$\frac{\partial \sigma_{rj}}{\partial r} + \frac{\sigma_{rj} - \sigma_{\theta j}}{r} + \frac{\partial \tau_{rzj}}{\partial z} = 0 \tag{27}$$

$$\frac{\partial \sigma_{zj}}{\partial z} + \frac{\partial \tau_{zrj}}{\partial r} + \frac{1}{r}\frac{\partial \tau_{\theta zj}}{\partial \theta} + \frac{1}{r}\tau_{rzj} = 0 \tag{28}$$

$$\varepsilon_{rj} - \phi_j(T) = \frac{1}{E_j(T)}\left[\sigma_{rj} - \upsilon_j(T)\left(\sigma_{\theta j} + \sigma_{zj}\right)\right] \tag{29}$$

$$\varepsilon_{\theta j} - \phi_j(T) = \frac{1}{E_j(T)}\left[\sigma_{\theta j} - \upsilon_j(T)\left(\sigma_{rj} + \sigma_{zj}\right)\right] \tag{30}$$

$$\varepsilon_{zj} - \phi_j(T) = \frac{1}{E_j(T)}\left[\sigma_{zj} - \upsilon_j(T)\left(\sigma_{\theta j} + \sigma_{rj}\right)\right] \tag{31}$$

$$\gamma_{rzj} = \frac{\tau_{rzj}}{G_j(T)} \tag{32}$$

$$\varepsilon_{rj} = \frac{\partial u_{rj}}{\partial r} \tag{33}$$

$$\varepsilon_{\theta j} = \frac{u_{rj}}{r} \tag{34}$$

$$\varepsilon_{zj} = \frac{\partial u_{zj}}{\partial z} \tag{35}$$

$$\gamma_{rzj} = \frac{\partial u_{rj}}{\partial z} + \frac{\partial u_{zj}}{\partial r} \tag{36}$$

The problem is also assumed to be a case of generalized plane strain. This means that shear stresses will be zero ($\tau_{rz} = \tau_{\theta z} = 0$). This affects Eqs. (27-36) in the following way.

$$\frac{\partial \sigma_{rj}}{\partial r} + \frac{\sigma_{rj} - \sigma_{\theta j}}{r} = 0 \tag{37}$$

$$\frac{\partial \sigma_{zj}}{\partial z} = 0 \tag{38}$$

$$\varepsilon_{rj} - \phi_j(T) = \frac{1}{E_j(T)}\left[\sigma_{rj} - \upsilon_j(T)\left(\sigma_{\theta j} + \sigma_{zj}\right)\right] \tag{39}$$

$$\varepsilon_{\theta j} - \phi_j(T) = \frac{1}{E_j(T)}\left[\sigma_{\theta j} - \upsilon_j(T)\left(\sigma_{rj} + \sigma_{zj}\right)\right] \tag{40}$$

$$\varepsilon_{zj} - \phi_j(T) = \frac{1}{E_j(T)}\left[\sigma_{zj} - \upsilon_j(T)\left(\sigma_{\theta j} + \sigma_{rj}\right)\right] \tag{41}$$

$$\varepsilon_{rj} = \frac{\partial u_{rj}}{\partial r} \tag{42}$$

$$\varepsilon_{\theta j} = \frac{u_{rj}}{r} \tag{43}$$

$$\varepsilon_{zj} = \frac{\partial u_{zj}}{\partial z} \tag{44}$$

$$\gamma_{rzj} = \frac{\partial u_{rj}}{\partial z} + \frac{\partial u_{zj}}{\partial r} = 0 \tag{45}$$

Furthermore, ε_z is assumed to be a constant value—that is to say that the composite cylinder will longitudinally elongate (or actually shrink in this case), but that it will do so by a constant amount. This assumption eliminates the system dependence on Eqs. (38, 45). While this simplifies the problem, it still introduces the need for another boundary condition as discussed below due to the fact that ε_z equals an unknown constant. Thus the equations change as follows:

$$\frac{\partial \sigma_{rj}}{\partial r} + \frac{\sigma_{rj} - \sigma_{\theta j}}{r} = 0 \tag{46}$$

$$\varepsilon_{rj} - \phi_j(T) = \frac{1}{E_j(T)}\left[\sigma_{rj} - \upsilon_j(T)\left(\sigma_{\theta j} + \sigma_{zj}\right)\right] \tag{47}$$

$$\varepsilon_{\theta j} - \phi_j(T) = \frac{1}{E_j(T)}\left[\sigma_{\theta j} - \upsilon_j(T)\left(\sigma_{rj} + \sigma_{zj}\right)\right] \tag{48}$$

$$\varepsilon_{zj} - \phi_j(T) = \frac{1}{E_j(T)}\left[\sigma_{zj} - \upsilon_j(T)\left(\sigma_{\theta j} + \sigma_{rj}\right)\right] \tag{49}$$

$$\varepsilon_{rj} = \frac{\partial u_{rj}}{\partial r} \tag{50}$$

$$\varepsilon_{\theta j} = \frac{u_{rj}}{r} \tag{51}$$

$$\varepsilon_{zj} = C \tag{52}$$

where C is a constant.

Equations (50-52) are substituted into Eqs. (47-49). This removes all the strain terms from the system.

$$\frac{\partial \sigma_{rj}}{\partial r} + \frac{\sigma_{rj} - \sigma_{\theta j}}{r} = 0 \tag{53}$$

$$\frac{\partial u_{rj}}{\partial r} - \phi_j(T) = \frac{1}{E_j(T)}\left[\sigma_{rj} - \upsilon_j(T)\left(\sigma_{\theta j} + \sigma_{zj}\right)\right] \tag{54}$$

$$\frac{u_{rj}}{r} - \phi_j(T) = \frac{1}{E_j(T)}\left[\sigma_{\theta j} - \upsilon_j(T)\left(\sigma_{rj} + \sigma_{zj}\right)\right] \tag{55}$$

$$C - \phi_j(T) = \frac{1}{E_j(T)}\left[\sigma_{zj} - \upsilon_j(T)\left(\sigma_{\theta j} + \sigma_{rj}\right)\right] \tag{56}$$

Equations (54-56) are solved simultaneously for the three stress terms (σ_r, σ_θ, and σ_z). The equations were solved using symbolic manipulation features of Maple 8 (Maplesoft, 2003).

$$\sigma_{rj}(r) = -\left(\frac{E_j(r)}{r\left(2\upsilon_j(r)^2 + \upsilon_j(r) - 1\right)}\right) \cdot \left(\left(\frac{du_{rj}}{dr}\right)\left(1 - \upsilon_j(r)\right)r + u_{rj} \cdot \upsilon_j(r) + r \cdot \upsilon_j(r) \cdot C - \phi_j(r) \cdot r\left(1 + \upsilon_j(r)\right)\right) \tag{57}$$

$$\sigma_{\theta j}(r) = -\left(\frac{E_j(r)}{r\left(2\upsilon_j(r)^2 + \upsilon_j(r) - 1\right)}\right) \cdot \left(\left(\frac{du_{rj}}{dr}\right)\upsilon_j(r) \cdot r + u_{rj}\left(1 - \upsilon_j(r)\right) + r \cdot \upsilon_j(r) \cdot C - \phi_j(r) \cdot r\left(1 + \upsilon_j(r)\right)\right) \tag{58}$$

$$\sigma_{zj}(r) = -\left(\frac{E_j(r)}{r\left(2\upsilon_j(r)^2 + \upsilon_j(r) - 1\right)}\right) \cdot \left(\left(\frac{du_{rj}}{dr}\right)\upsilon_j(r) \cdot r + u_{rj} \cdot \upsilon_j(r) + C \cdot r\left(1 - \upsilon_j(r)\right) - \phi_j(r) \cdot r\left(1 + \upsilon_j(r)\right)\right) \tag{59}$$

By substituting the stresses in terms of displacements (Eqs. (57-59)) into Eq. (53), the equilibrium equation is rewritten in terms of displacements only. This final substitution is lengthy and was also done by using Maple. The result was organized by grouping terms which contained a second derivative of radial displacement, a first derivative of radial displacement, radial displacement, and the constant C. Thus the long

result of writing the equilibrium equation in terms of only radial displacements can be expressed in this form:

$$D_{1j}(r)\frac{d^2u_{rj}}{dr^2}+D_{2j}(r)\frac{du_{rj}}{dr}+D_{3j}(r)\cdot u_{rj}+D_{4j}(r)\cdot C+D_{5j}(r)=0 \tag{60}$$

where D_1, D_2, D_3, D_4, and D_5 are all coefficients made up of material properties and are functions of radial location. They have also been simplified by using Maple. As a further precaution, the code generator option of Maple was used to generate the FORTRAN code from the simplified Maple equations. The following are the coefficient functions:

$$D_{1j}(r)=\frac{E_j(r)(\upsilon_j(r)-1)}{2\upsilon_j(r)^2+\upsilon_j(r)-1} \tag{61}$$

$$\begin{aligned}D_{2j}(r)=&-\frac{\left(\frac{dE_j(r)}{dr}\right)\left(-2\upsilon_j(r)^3+\upsilon_j(r)^2-2\upsilon_j(r)-1\right)}{\left(2\upsilon_j(r)^2+\upsilon_j(r)-1\right)}\\&-\frac{E_j(r)\left(\frac{d\upsilon_j(r)}{dr}\right)\left(2\upsilon_j(r)^2-4\upsilon_j(r)\right)}{\left(2\upsilon_j(r)^2+\upsilon_j(r)-1\right)}\\&-\frac{E_j(r)\left(-2\upsilon_j(r)^3+\upsilon_j(r)^2+2\upsilon_j(r)-1\right)}{r\left(2\upsilon_j(r)^2+\upsilon_j(r)-1\right)}\end{aligned} \tag{62}$$

$$\begin{aligned}D_{3j}(r)=&\frac{\left(\frac{dE_j(r)}{dr}\right)\left(-2\upsilon_j(r)^3-\upsilon_j(r)^2+\upsilon_j(r)\right)}{r\left(2\upsilon_j(r)^2+\upsilon_j(r)-1\right)^2}+\frac{E_j(r)\left(\frac{d\upsilon_j(r)}{dr}\right)\left(2\upsilon_j(r)^2+1\right)}{r\left(2\upsilon_j(r)^2+\upsilon_j(r)-1\right)^2}\\&+\frac{E_j(r)\left(-2\upsilon_j(r)^3+\upsilon_j(r)^2+2\upsilon_j(r)-1\right)}{r^2\left(2\upsilon_j(r)^2+\upsilon_j(r)-1\right)^2}\end{aligned} \tag{63}$$

$$D_{4j}(r)=-\frac{\left(\frac{dE_j(r)}{dr}\right)\left(2\upsilon_j(r)^3+\upsilon_j(r)^2-\upsilon_j(r)\right)}{\left(2\upsilon_j(r)^2+\upsilon_j(r)-1\right)^2}-\frac{E_j(r)\left(\frac{d\upsilon_j(r)}{dr}\right)\left(2\upsilon_j(r)^2+1\right)}{\left(2\upsilon_j(r)^2+\upsilon_j(r)-1\right)^2} \tag{64}$$

$$D_{5j}(r)=\frac{\phi_j(r)\left(\frac{dE_j(r)}{dr}\right)}{\left(2\upsilon_j(r)-1\right)}+\frac{E_j(r)\left(\frac{d\phi_j(r)}{dr}\right)}{\left(2\upsilon_j(r)-1\right)}+\frac{2\cdot E_j(r)\cdot\phi_j(r)\left(\frac{d\upsilon_j(r)}{dr}\right)}{\left(2\upsilon_j(r)-1\right)^2} \tag{65}$$

Note that the material properties are shown to be functions of radius when in reality they are functions of temperature. In this study, the temperature at each time step is a function of radius. For simplicity, the material properties are shown as functions of radius. When a material property was calculated, the radius input was used to calculate the corresponding temperature at that point and the property was evaluated at said temperature.

As with the thermal formulation, the material properties are functions of temperature and must be kept as functions and not constants. Note in Figure 7 how the coefficient of thermal expansion varies over the specified temperature range.

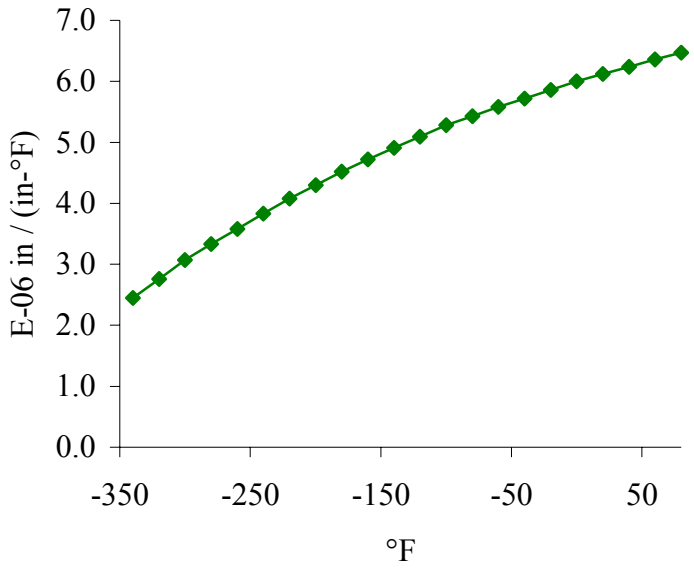

Figure 7. Coefficient of Thermal Expansion as a Function of Temperature

Equation (60) was used for all interior nodes in both cylinders. Care must be taken to keep the material properties of each cylinder completely separate. The derivatives of u_r were approximated using the following second order accurate central approximations:

$$\frac{d^2 u_{rj}}{dr^2} = \frac{1}{\Delta r_j^{\,2}}\left(u_{rj,-1} - 2\cdot u_{rj,0} + u_{rj,1}\right) \tag{66}$$

$$\frac{du_{rj}}{dr} = \frac{1}{2\cdot \Delta r_j}\left(-u_{rj,-1} + u_{rj,1}\right) \tag{67}$$

In Eqs. (62-65) there are derivatives of material properties. The material properties used are discrete data points given in Appendix 1. These data points were interpolated using cubic splines. The derivatives were obtained using second order accurate central approximations.

Elasticity Boundary Conditions

The loads in this problem are the stresses due to the interface and the thermal stresses. Due to the absence of other external loads acting on the composite cylinder, the radial stress on the inner and outer edges must be zero. The inner radius ($r = a$) of Cylinder 1 was substituted into the expression found for the radial stress in terms of displacements only, Eq. (57). The outer radius ($r = c$) of Cylinder 2 was also substituted into Eq. (57). The radial stress term has a first derivative of u_r in it which requires approximating. As before in the case of the thermal boundary conditions, a forward approximation was used for the inner edge and a backward approximation for the outer edge.

$$\sigma_{r1}(a) = 0 \tag{68}$$

$$-\left(\frac{E_1(a)}{a\left(2\upsilon_1(a)^2 + \upsilon_1(a) - 1\right)}\right) \cdot \left(\left(\frac{du_{r1}}{dr}\right)\left(1 - \upsilon_1(a)\right)a + u_{r1_0} \cdot \upsilon_1(a) + a \cdot \upsilon_1(a) \cdot C - \phi_1(a) \cdot a\left(1 + \upsilon_1(a)\right)\right) = 0 \tag{69}$$

and

$$\sigma_{r2}(c) = 0 \tag{70}$$

$$-\left(\frac{E_2(c)}{a\left(2\upsilon_2(c)^2 + \upsilon_2(c) - 1\right)}\right) \cdot \left(\left(\frac{du_{r2}}{dr}\right)\left(1 - \upsilon_2(c)\right)c + u_{r2_M} \cdot \upsilon_2(c) + c \cdot \upsilon_2(c) \cdot C - \phi_2(c) \cdot c\left(1 + \upsilon_2(c)\right)\right) = 0 \tag{71}$$

The two interface conditions, as with the thermal boundary conditions, come from the conditions of the interface at r = b. In the thermal case, the temperatures and flux at node N of cylinder 1 and node 0 of cylinder 2 were equal. This does not correspond to the displacements. The inner cylinder was originally too large for the outer cylinder, and so it was shrunk into the outer cylinder. This causes an interference which is based on just how tight a fit is needed. The displacements at the interface nodes (node N of cylinder 1 and node 0 of cylinder 2) will differ by a specified factor of this interference, denoted by δ.

$$u_{r1_N} - u_{r2_0} = \delta \tag{72}$$

The remaining boundary condition is that the radial stresses must be equal at the interface as well. Again, Eq. (57) is used because it represents the radial stress in terms of displacements only.

$$\sigma_{r1}(b) = \sigma_{r2}(b) \tag{73}$$

$$\begin{aligned}
&\left(\frac{E_1(b)}{b\left(2\upsilon_1(b)^2 + \upsilon_1(b) - 1\right)}\right)\cdot \\
&\left(\left(\frac{du_{r1}}{dr}\right)\left(1-\upsilon_1(b)\right)b + u_{r1_0}\upsilon_1(b) + b\cdot\upsilon_1(b)\cdot C - \phi_1(b)\cdot b\left(1+\upsilon_1(b)\right)\right) \\
&= \left(\frac{E_2(b)}{b\left(2\upsilon_2(b)^2 + \upsilon_2(b) - 1\right)}\right)\cdot \\
&\left(\left(\frac{du_{r2}}{dr}\right)\left(1-\upsilon_2(b)\right)b + u_{r2_M}\upsilon_2(b) + b\cdot\upsilon_2(b)\cdot C - \phi_2(b)\cdot b\left(1+\upsilon_2(b)\right)\right)
\end{aligned} \tag{74}$$

As stated before with the thermal portion, two separate systems of differential equations are being solved, linked by boundary conditions. There are second derivatives in each cylinder so a total of four boundary conditions are needed, two for each cylinder. The derivatives in all of these equations are discretized using the above mentioned methods. What results is another system of linear equations where the unknowns are displacements at various nodes. It would appear that the problem is ready to be solved, but another equation is needed.

In Eq. (52) it was stated that ε_z is equal to a constant C. The purpose of leaving ε_z a constant was to be more accurate, allowing for the cylinder to contract longitudinally a constant amount. This introduces another unknown into the problem, for which another equation is needed. Although the composite cylinder will contract, there will be no force acting on the face. By summing up the force on the face of the composite cylinder and setting it equal to zero, we develop another equation for finding the value of C.

$$\int_a^b 2\pi r\sigma_{z1}dr + \int_b^c 2\pi r\sigma_{z2}dr = 0 \tag{75}$$

The area multiplied by the stress, σ_z over the entire area of the end of the cylinder is the force. The expression for σ_z in terms of only radial displacements is used. The constant is not immediately seen in the formula, but is part of the expression for σ_z. For the assumption of $\varepsilon_z = C$ to be possible, this condition must be satisfied. Equation (59) was used to express the longitudinal stress because it is in terms of displacements only.

Satisfying this boundary condition proved to be the most difficult aspect of the program. The problem consists in this: σ_z is a large expression which contains radial displacement terms. The very unknowns being solved for are inside the integral. To solve this problem, the integrals were approximated using multiple-segment Simpson's 1/3 Rule (Chapra, 1998). They were expanded and like terms were collected.

This completes another system of linear equations which is solved simultaneously to calculate the displacement at each node. These displacements were substituted into Eqs. (57-59) to get the value of the stresses at each node. The next section details how the stress values are used to predict failure.

Failure Criteria

The purpose of the study was to compare cooling procedures, not to find exact stresses. The stresses calculated determine if and when the cylinder fails. This quantifies how well different cooling methods function. This study based failure on two quantities: the overall minimum stress ratio and the overall minimum critical crack length. As the cylinders get colder, there is an increased chance that they will crack. It is also possible that the transient stress values exceed the allowable. That is why both criteria are being examined.

The stress ratio is a comparison of the Von Mises stress with the yield stress. It can also be viewed as the factor of safety. Failure occurs when the stress ratio falls below one (i.e. the Von Mises stresses become larger that the yield stress). The following formula was used (Timoshenko, 1951).

$$SR = \frac{\sigma_{YS}(T)}{\sqrt{\sigma_r^2 + \sigma_\theta^2 - 2 \cdot \sigma_r \cdot \sigma_\theta}} \tag{76}$$

where,

SR is the stress ratio,

and σ_{YS} is the yield strength of the material.

Yield strength is not a constant value, but a function of temperature. Therefore, the Von Mises stress is calculated from the radial and hoop stresses at each node and compared to the yield strength at the particular temperature of said node. For a given time step, the minimum stress ratio was found in the cylinder wall. That minimum stress ratio was compared to the minimum stress ratio of the previous time step. Only the lowest stress ratio was stored. The stress ratio that is ultimately generated is then a worst case stress ratio because it is the lowest in space and time. For this study, it was desired to know what the lowest stress ratio was and where on the two cylinders did it occur.

The critical crack length is defined as the crack length after which failure occurs. The formula involves another physical property called fracture toughness. In most instances, the critical crack is a specified length based on what kind of equipment is being used for inspection. Based on that crack length and the fracture toughness of the material,

a stress level can be found after which failure is assumed to occur. The following formula is used to determine that stress level (Kanninen, 1985).

$$\sigma_{crack} = \frac{K_{IC}(T)}{1.25\sqrt{\pi L_{crack}}} \tag{77}$$

where,

σ_{crack} is the hoop stress after which failure occurs,

K_{IC} is the fracture toughness of the material, and

L_{crack} is the length of the smallest detectable crack in the assembly.

In this study, the actual stress as well as the fracture toughness is known. The stress used is the hoop stress at a specific point and the fracture toughness is evaluated at the temperature at that point. Thus the formula is rearranged to show the length of the critical crack.

$$L_{crack} = \frac{\left(\frac{K_{IC}}{1.25\sigma_{crack}}\right)^2}{\pi} \tag{78}$$

What this is interpreted to mean is that any crack larger than this length will produce failure. As with the overall minimum stress ratio, the overall minimum critical crack length is the absolute minimum crack length in time and space for the cylinder. This overall minimum crack length was recorded as well as the location it occurred.

Both failure criteria are implemented because it is not known exactly what the cause of failure is. As the cylinder cools down, the yield strength increases which makes the stress ratio higher yet the fracture toughness drops making the cylinder more susceptible to cracking. Figure 8 shows a graph of the fracture toughness and yield strength as a function of temperature.

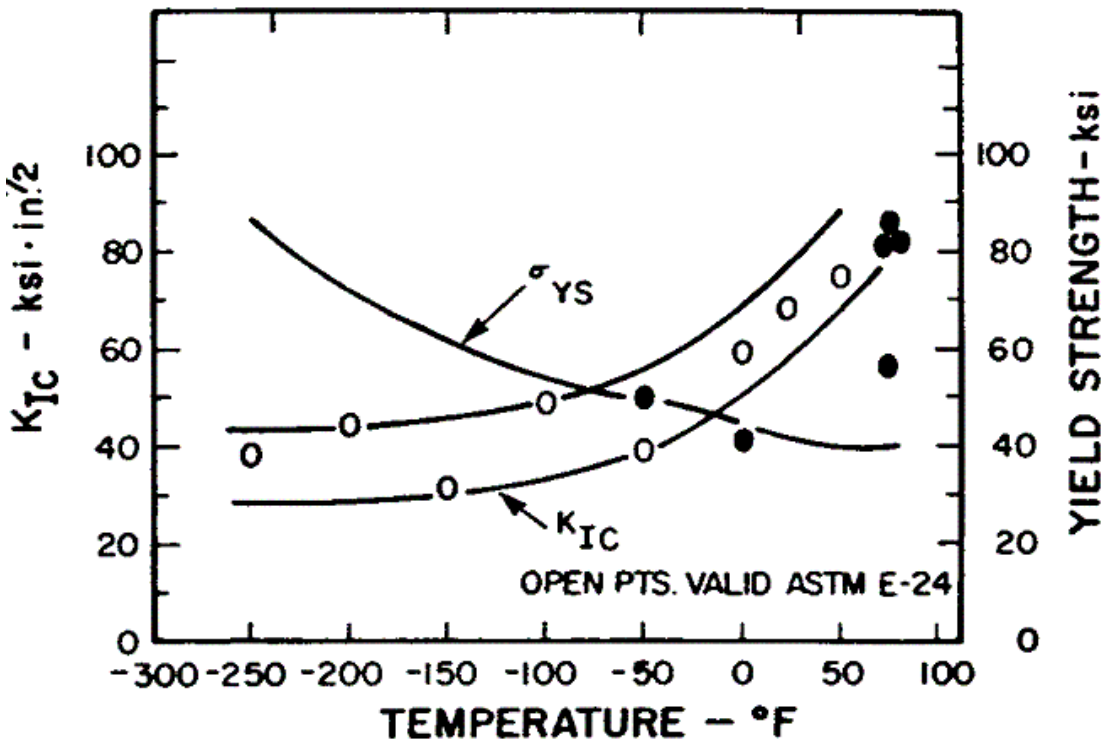

Figure 8. Fracture Toughness and Yield Strength as a Function of Temperature (Source: Greenberg, 1969)

CHAPTER 3 – RESULTS

The concepts presented in the previous chapter were implemented to write a program in FORTRAN. Although the program allows for infinite number of cases to be run, three cases were taken into consideration for this thesis. Although each bridge has many important parameters, for this study we are merely interested in the geometric parameters listed in Table 1. For clarification, Fig. 9 shows the correlation of these dimensions to the actual body.

Table 1. Geometric Data for the Three Bridges

Geometric Parameters	Bridge		
	Christa McAuliffe	Hillsborough Avenue	17th Street Causeway
a - in	1.0	1.125	1.1875
b - in	9.0	8.39	6.472
c - in	16.0	15.39	8.88

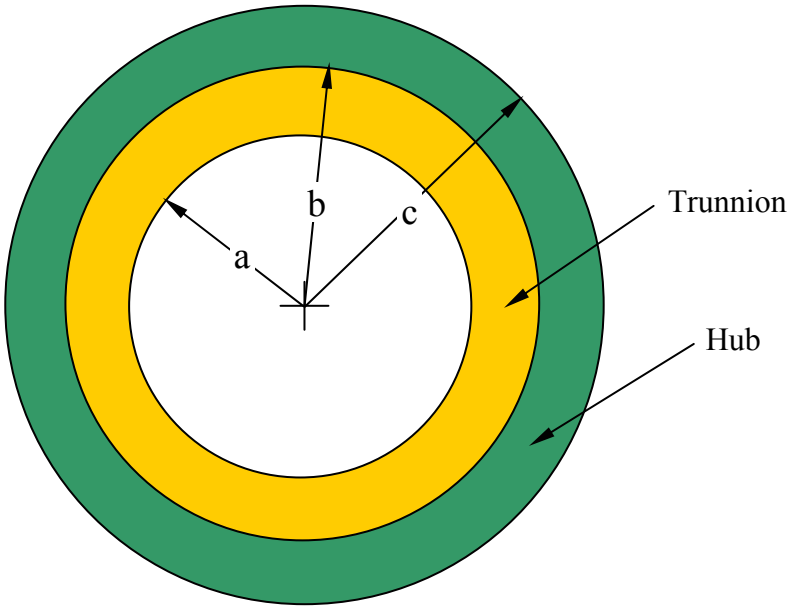

Figure 9. Geometry of Trunnion-Hub Assembly

It can be seen from Table 1 that the dimensions of the girder and hub assembly can vary a large amount. According to the original research statement produced by FDOT, hub thicknesses ($c - b$) can range from 1.5 inches to 8 inches. The trunnion dimensions are less flexible because they must meet certain criteria for the bridge. The hub thickness, however, is more arbitrary. While AASHTO Specifications (AASHTO, 1998) call for a hub thickness of 0.4 times the diameter (in this case $0.4 \cdot 2b$), the standard practice in industry is to use a hub thickness of $(0.1 \text{ to } 0.2) \cdot 2b$ (Request for Proposal, 1998). The hub thickness has a great effect on the thermal behavior of the assembly. To see the effect of the hub thickness, the trunnion dimensions (*a* and *b*) of each bridge were used and the outer dimension (which controls the hub thickness) was varied from $(0.1 \text{ to } 0.4) \cdot 2b + b$. This was done for each of the three bridges as well as for each of the three cooling methods. For each bridge configuration and cooling method the overall minimum critical crack length and stress ratio were recorded. The results of that study are given below.

Some comment should be made on the organization of the data. The cylinders have an interface fit, specifically a standard interface fit called FN2. If the trunnion is fit into the hub, there is an upper and lower limit by which the outer diameter of the trunnion and the inner diameter of the hub vary. These limits are calculated using the following expression (Shigley, 1986).

$$L_{FN2} = C_{FN2} \cdot D_{FN2}{}^{\frac{1}{3}} \tag{79}$$

where,

L_{FN2} is the limit in thousandths of an inch,

C_{FN2} is a constant specified in the table below,

and D_{FN2} is the cylinder diameter in inches.

Table 2. Constants C_{FN2} Used in Finding Cylinder Tolerances

Class of fit	Cylinder A (hub)		Cylinder B (trunnion)	
	Lower	Upper	Lower	Upper
FN2	0	0.907	2.717	3.288

The limits for the Trunnion-Hub used on the Christa McAuliffe Bridge are calculated using its radius $b = 9\,\text{in}$ (See Table 1), Eq. (79), and the constants listed in Table 2.

$$L_{FN2} = 0 \cdot (2 \cdot 9)^{\frac{1}{3}} = 0\,\text{in} \tag{80}$$

$$L_{FN2} = 0.907 \cdot (2 \cdot 9)^{\frac{1}{3}} = 0.002377\,\text{in} \tag{81}$$

$$L_{FN2} = 2.717 \cdot (2 \cdot 9)^{\frac{1}{3}} = 0.007121\,\text{in} \tag{82}$$

$$L_{FN2} = 3.288 \cdot (2 \cdot 9)^{\frac{1}{3}} = 0.008617\,\text{in} \tag{83}$$

The outer diameter of the trunnion, according to the standard for FN2 fits, is $18^{+0.008617}_{+0.007121}$ inches and the inner diameter of the hub is $18^{+0.002377}_{+0.000000}$ inches. The difference between the inner diameter of the hub and the outer diameter of the trunnion is called the interference and is denoted as δ. The interference will have a high and low limit. These limits are found by subtracting the diameters at their extremes.

$$\delta = 18.008617 - 18.0 = 0.008617 \text{ in} \tag{84}$$

$$\delta = 18.008617 - 18.002377 = 0.006240 \text{ in} \tag{85}$$

$$\delta = 18.007121 - 18.0 = 0.007121 \text{ in} \tag{86}$$

$$\delta = 18.007121 - 18.002377 = 0.004744 \text{ in} \tag{87}$$

Equations (84-87) show that the diametric interference is as much as 0.008617 inches and as little as 0.004744 inches. These limits are small, but significant. In this study, the interface stress is the main source of stress within the body. For this reason, each bridge configuration and cooling method was run twice, once at the high end of the diametrical interface limit and once at the low end.

Thus the outer radius of Cylinder 2, the diametrical interface, and the cooling process were varied, the program run, and the overall minimum critical crack and overall minimum stress ratio recorded. As mentioned in the introduction and repeated here for convenience, the three cooling processes considered are the following:

- Process 1 - Direct immersion into liquid nitrogen
- Process 2 - Immersion into a refrigerated chamber, then liquid nitrogen
- Process 3 - Immersion into a refrigerated chamber, then a dry-ice/alcohol bath, and finally liquid nitrogen

The following are the results from the Christa McAuliffe Bridge.

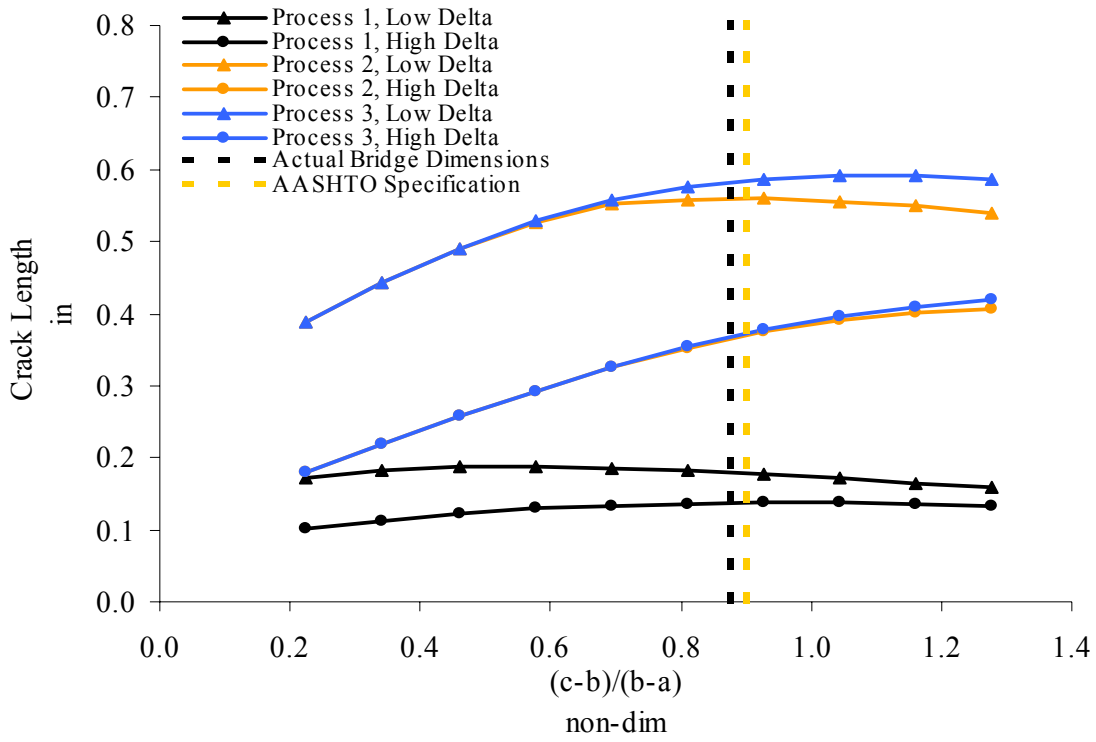

Figure 10. Overall Minimum Critical Crack Length as a Function of Hub-Trunnion Thickness Ratio for the Christa McAuliffe Bridge

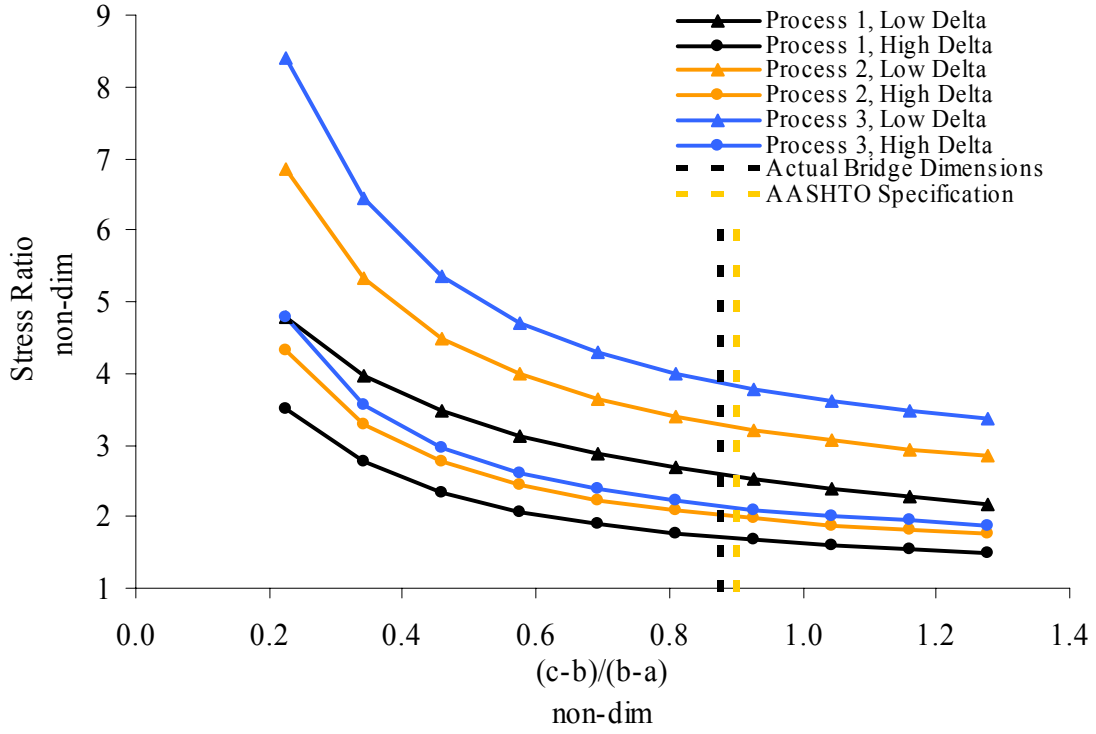

Figure 11. Overall Minimum Stress Ratio as a Function of Hub-Trunnion Thickness Ratio for the Christa McAuliffe Bridge

Figures 10 and 11 show the overall minimum critical crack length and the overall minimum stress ratio, respectively. In Figure 10, the overall minimum critical crack length is plotted versus the hub-trunnion thickness ratio. Note the curves representing Process 1. The overall minimum critical crack length is low for the full range of hub-trunnion thickness ratio. The crack length varies slightly from high interface values to low interface values. The curves representing Process 2 indicate an overall minimum critical crack length that is on average 150% longer. Not only that, but the crack length varies three times as much from high to interface values as in process one. Adding a refrigerated air stage has definite advantages. Note the curves representing Process 3. The usefulness of adding a cooling stage of dry-ice/alcohol is limited. Process 3 only adds on average an additional 1% of benefit to process two.

In Figure 11, the effect of adding a stage of dry-ice/alcohol can be more clearly seen. Process 2 increases the overall minimum stress ratio by an average of 20% and Process 3 increases it by an additional 7%. Although the overall minimum stress ratio does not fall below one in these experiments, for larger hub-trunnion thickness ratios it does become as low as 1.5.

The actual bridge configuration and the AASHTO specifications can be seen in Figures 10 and 11 by vertical lines. This shows that the Christa McAuliffe was designed following the AASHTO standards and where the overall minimum critical crack length was about 0.15 inches.

Figures 12 and 13 show the same results for the Hillsborough St. Bridge. The trunnion-hub assembly of this bridge is similar in size to the Christa McAuliffe (see Table 1) and therefore the results are similar. Figures 14 and 15 show results for the 17th Ave. Causeway Bridge, whose trunnion-hub assembly is roughly half the size of the other two bridges considered. Figure 14 shows almost no benefit to adding the dry-ice/alcohol as a cooling stage. This is most likely due to the fact that the rate at which heat is convected into the fluid is partially based on the diameter of the cylinder. Since the 17th Ave. Causeway is half the size of the others, its convection coefficient is smaller and therefore does not make a significant contribution. This can also be seen in Figures 10 and 12 when the hub-trunnion thickness ratio is smaller.

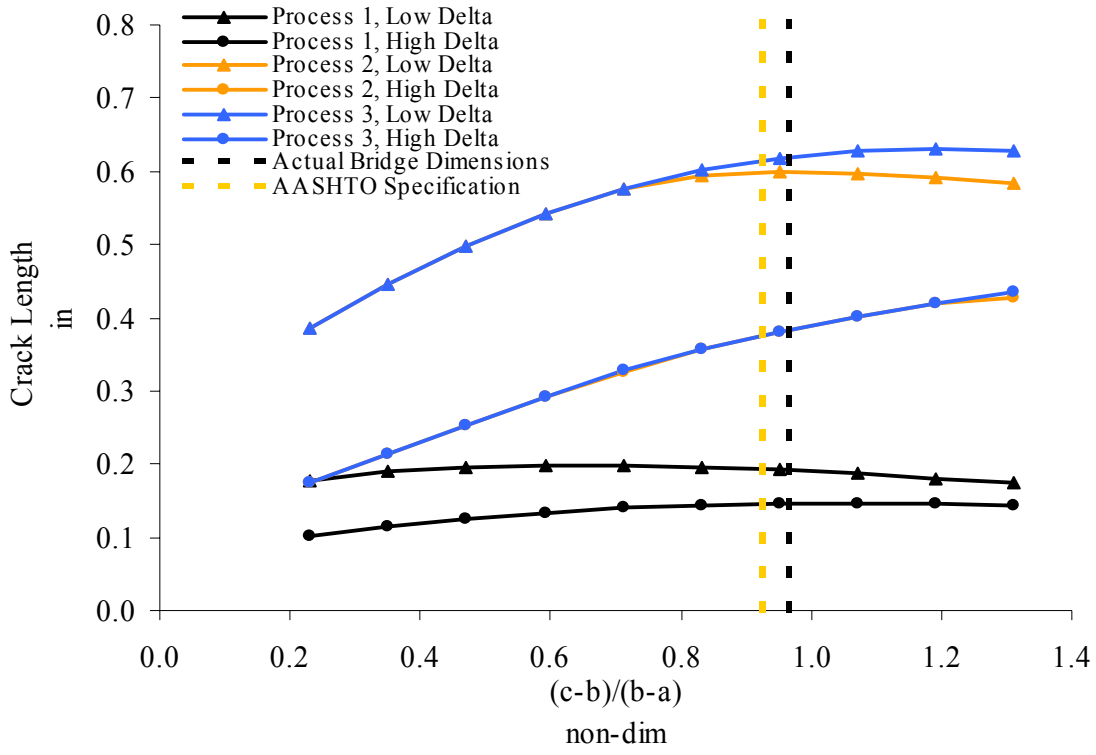

Figure 12. Overall Minimum Critical Crack Length as a Function of Hub-Trunnion Thickness Ratio for the Hillsborough Ave. Bridge

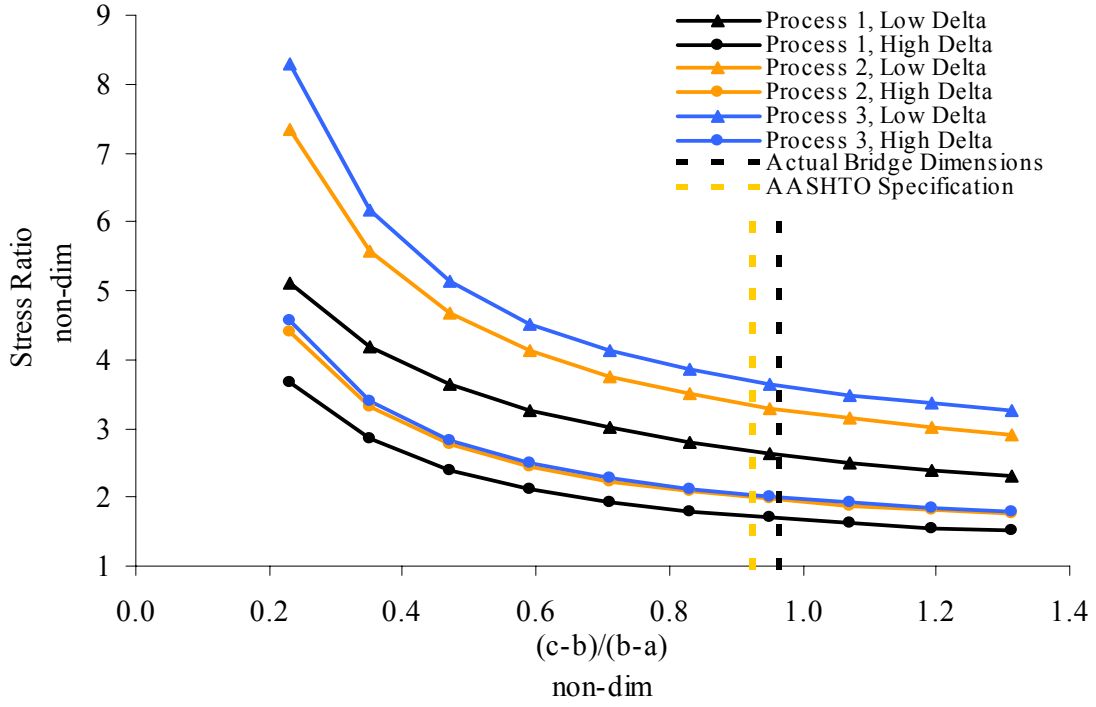

Figure 13. Overall Minimum Stress Ratio as a Function of Hub-Trunnion Thickness Ratio for the Hillsborough Ave. Bridge

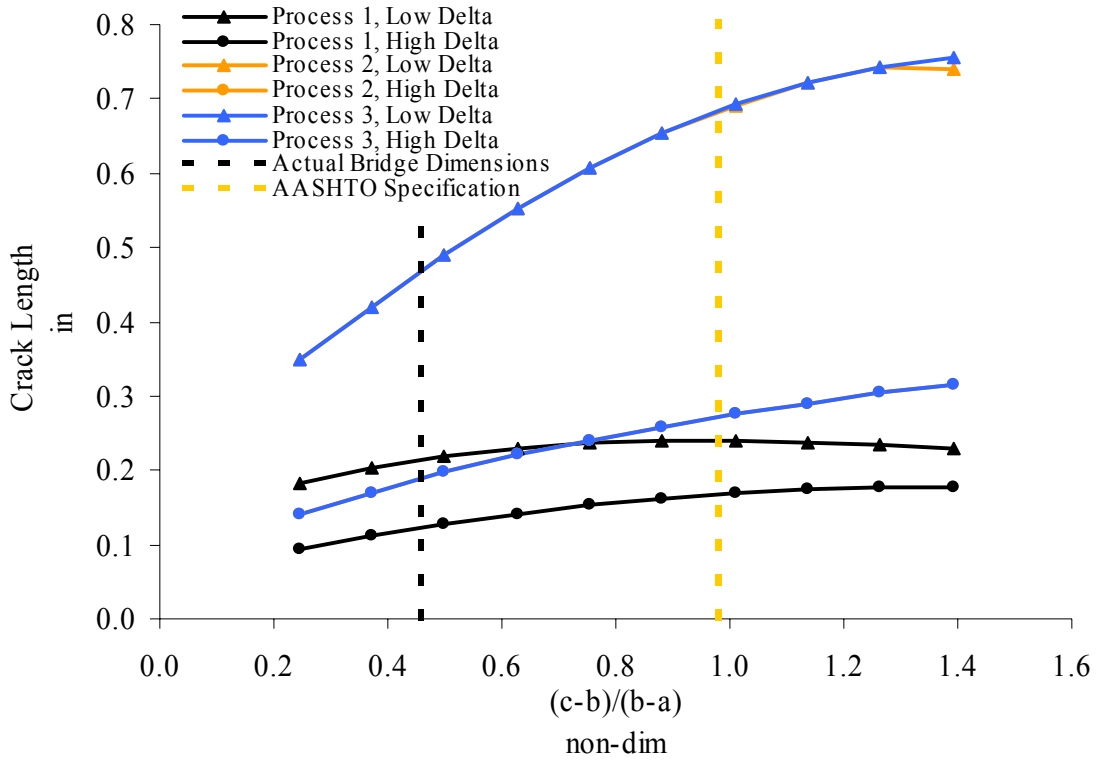

Figure 14. Overall Minimum Critical Crack Length as a Function of Hub-Trunnion Thickness Ratio for the 17th St. Causeway Bridge

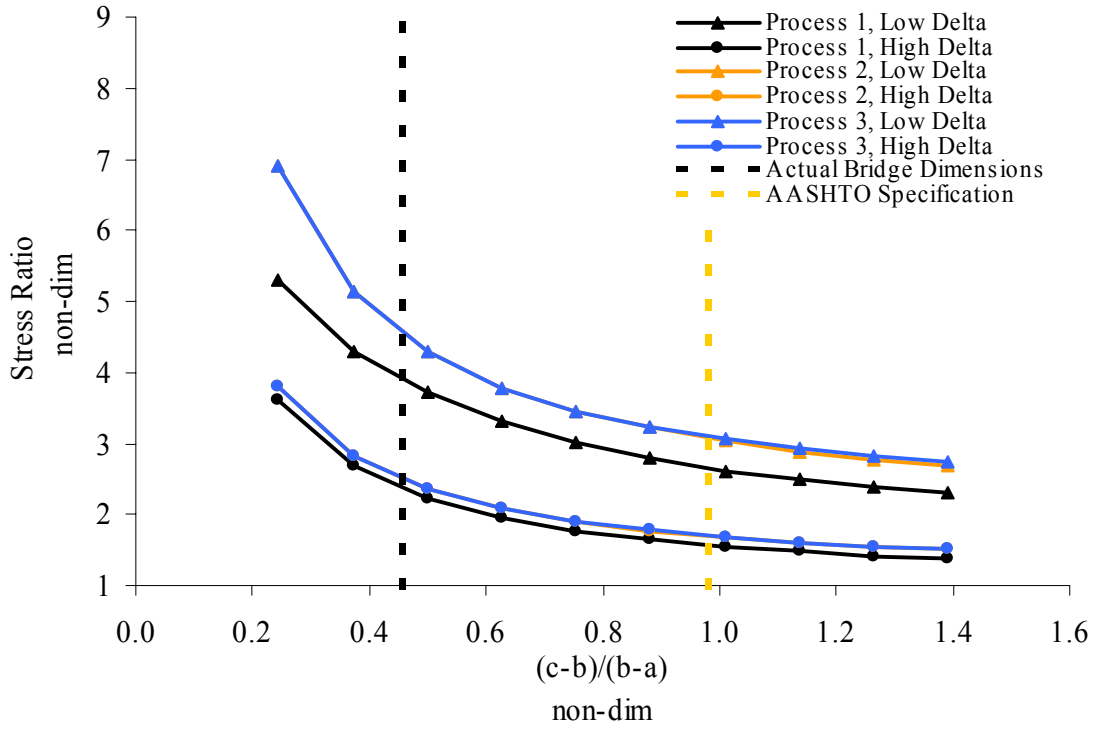

Figure 15. Overall Minimum Stress Ratio as a Function of Hub-Trunnion Thickness Ratio for the 17th St. Causeway Bridge

Conclusions

As expected, Processes 2 and 3 have a definite advantage over a range of thickness ratios and bridge sizes. A curious result is that Process 3 did not yield significantly improved results from Process 2. However, at higher diameters (the 17th Street Causeway Bridge is smaller than the other two) the effect of the dry-ice/alcohol from Process 3 is seen, but it does not seem to grant a high level of benefit. The benefit it does give is to the upper end of the critical crack length. This does not improve the worst case scenario (the lower end). Of course this information is based on the quality of the property data used, but it does suggest that pre-refrigerating is recommended as it is relatively cheap and an easy procedure to perform.

The graphs also depict the effect of the hub-trunnion thickness ratio in assembly process. Making the hub-trunnion thickness ratio larger is good for the increasing the overall minimum critical crack length, but has the opposite effect on the overall minimum stress ratio. Although the stress ratio never falls below unacceptable values in these numerical experiments, it does approach its low limit of one at high values of hub-trunnion thickness ratio. Thus, a trade off similar to the one between fracture toughness and yield strength occurs.

Staged cooling not only raises the overall minimum critical crack length and stress ratio, it also increases the gap between the minimum and maximum possible values. This is not necessarily an improvement. However, as the difference between minimum and maximum values increases, the greater the statistical chance that the actual value will be further from an extreme.

In addition to the information graphed, the location of the overall minimum stress ratio and critical crack length was recorded. The values can be viewed in Appendix 6. A couple of interesting observations can be made. The minimum stress ratio always falls on the inside surface of Cylinder 1. This suggests that the use of a material with a higher yield strength for the trunnion is of benefit.

The overall minimum critical crack length most often falls on the outside surface of Cylinder 2, but geometries it fell on the inner surface of Cylinder 2 (at the interface). This poses another problem because cracks on the interface cannot be easily detected. A

cylinder can visually pass a crack test, but fail due to unseen cracks at the interface. This seems to happen in a few data points at high interface values on the smaller cylinders when the thickness ratio is high. Therefore, smaller cylinders with high interface stress and thickness ratio are more likely to have the crack at the interface instead of the outer surface. This phenomenon does not occur for low interference values or in the larger THG geometries.

REFERENCES

AASHTO Mobile Bridge Inspection, Evaluation, and Maintenance Manual, 1998.

AspenTech, "Aspen Plus", [online] http://www.aspentech.com/, (Accessed 03/31/2004).

Barron, R. F., 1999, *Cryogenic Heat Transfer*, Taylor & Francis, Ann Arbor.

Boresi, A. P., and Chong, K.P., 1991, *Approximate Solution Methods in Engineering Mechanics,* Elsevier Applied Science Publishers LTD. New York, pp. 51-53.

Chapra, S. C., and Canale R. P., 1998, *Numerical Methods for Engineers,* WCB McGraw-Hill, New York.

Denninger, M.T., 2000, "Design Tools for Trunnion-Hub Assemblies for Bascule Bridges." MS Thesis, Mechanical Engineering Department, University of South Florida, FL.

Greenberg, H.D., and Clark, Jr. H.G., 1969, "A Fracture Mechanics Approach to the Development of Realistic Acceptance Standards for Heavy Walled Steel Castings", Metals Engineering Quarterly, 9(3), 30-33.

Incropera, F. P., and DeWitt, D.P., 1996, *Introduction to Heat Transfer*, John Wiley & Sons, Inc., NewYork.

Kakaç, S., and Yener Y., 1995, *Convective Heat Transfer*, CRC Press, Inc., Boca Raton.

Kanninen, M. F. and Popelar, C. H., 1985, *Advanced Fracture Mechanics*, Oxford Engineering Science Series, Oxford University Press, New York.

Kreith, F., and Bohn, M., 1986, *Principles of Heat Transfer*, Harper & Row, New York, pp. 98.

Logan, D. L., 1992, *A First Course in Finite Element Method*, *PWS-KENT Series in Engineering*, PWS-KENT Publishing Company, Boston.

Maplesoft, 2003, "Maple 9.0: Command the Brillance", [online] http://www.maplesoft.com/, (Accessed on 3/30/2004).

Nichani, S., 2001, "Full Scale Testing of Trunnion-Hub-Girder Assembly of a Bascule Bridge." MS Thesis, Mechanical Engineering Department, University of South Florida, FL.

Özişik, M. N., 1993, *Heat Conduction*, John Wiley & Sons, Inc., NewYork, pp. 8, 491.

Ratnam, B., 2000, "Parametric Finite Element modeling of trunnion Hub Girder Assemblies for Bascule Bridges." MS Thesis, Mechanical Engineering Department, University of South Florida, FL.

Request for Proposals for Parametric Finite Element Analysis of Trunnion-Hub Assemblies for Bascule Bridges, February 11, 1998, Florida Department of Transportation.

Shigley, J.E., and Mischke, 1986, *Standard Handbook of Machine Design*, McGraw-Hill, New York.

Timoshenko, S. P., and Goodier, J. N., 1951, *Theory of Elasticty*, McGraw-Hill Book Company, New York. pp. 406-408.

APPENDICES

Appendix 1: Property Data for Cylinder Material

The following tables detail the properties used in this experiment. Although this is not always the exact steel used in the THG assembly, the numbers are representative of the steels one would encounter.

Table A1. Elastic Properties of Steel as a Function of Temperature

Fe - 2.25 Ni (ASTM A203-A), Normalized				
Temperature	Young's Modulus	Poisson's Ratio	Tensile Strength	Tensile Yield Strength
°F	Msi	non-dim	ksi	ksi
-340.00	31.490	0.2756	115.0	102.0
-320.00	31.440	0.2758	111.0	95.0
-300.00	31.380	0.2760	108.0	89.0
-280.00	31.320	0.2763	105.0	83.0
-260.00	31.260	0.2765	102.0	78.0
-240.00	31.200	0.2768	99.0	73.0
-220.00	31.140	0.2770	96.0	68.0
-200.00	31.070	0.2773	93.5	64.0
-180.00	30.990	0.2776	91.0	60.5
-160.00	30.910	0.2779	89.0	58.0
-140.00	30.830	0.2781	87.0	56.0
-120.00	30.750	0.2784	85.0	54.0
-100.00	30.670	0.2787	83.0	52.0
-80.00	30.590	0.2790	81.0	50.5
-60.00	30.500	0.2793	79.0	49.0
-40.00	30.410	0.2796	77.0	48.0
-20.00	30.320	0.2799	75.5	47.5
0.00	30.230	0.2802	74.0	47.0
20.00	30.140	0.2805	73.0	47.0
40.00	30.050	0.2808	72.0	47.0
60.00	29.960	0.2811	71.0	47.0
80.00	29.870	0.2815	70.0	47.0

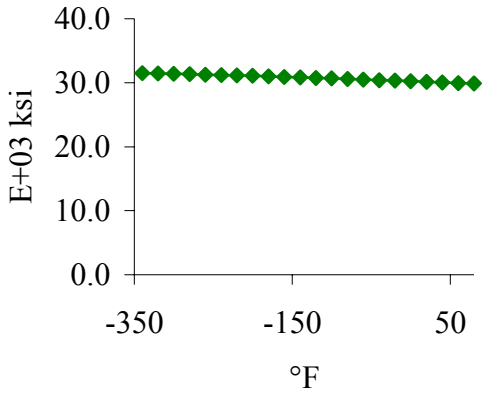

Figure A1. Young's Modulus of ASTM A203-A Steel as a Function of Temperature

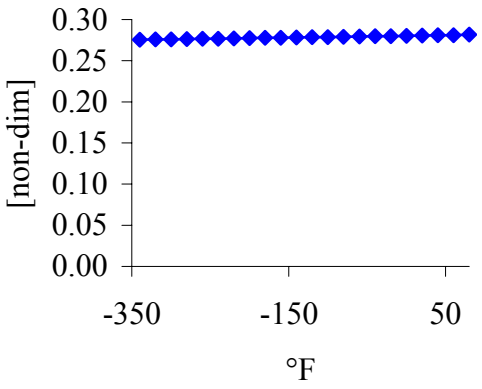

Figure A2. Poisson's Ratio of ASTM A203-A Steel as a Function of Temperature

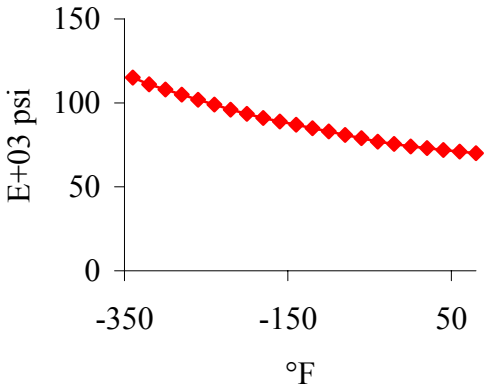

Figure A3. Tensile Strength of ASTM A203-A Steel as a Function of Temperature

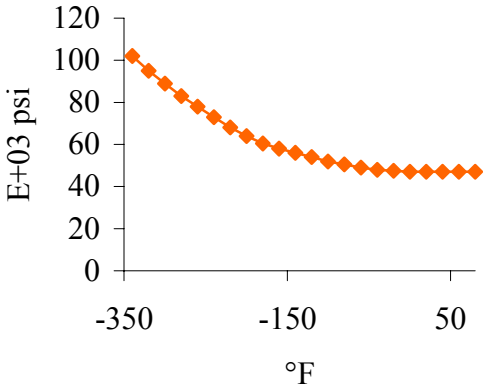

Figure A4. Yield Strength of ASTM A203-A Steel as a Function of Temperature

Table A2. Thermal Properties of Steel as a Function of Temperature

Fe - 2.25 Ni (ASTM A203-A), Normalized				
Temperature	Thermal Conductivity	Specific Heat	Density	Thermal Expansion
°F	BTU / (sec-in-°F)	BTU / (lbm-°F)	lb / in^3	$x10^{-6}$ in / (in-°F)
-340.00	0.0002825	0.0250	0.284	2.450
-320.00	0.0002939	0.0360	0.284	2.760
-300.00	0.0003103	0.0460	0.284	3.070
-280.00	0.0003306	0.0535	0.284	3.330
-260.00	0.0003508	0.0605	0.284	3.580
-240.00	0.0003714	0.0670	0.284	3.830
-220.00	0.0003917	0.0720	0.284	4.080
-200.00	0.0004097	0.0770	0.284	4.300
-180.00	0.0004244	0.0810	0.284	4.520
-160.00	0.0004369	0.0850	0.284	4.720
-140.00	0.0004494	0.0890	0.284	4.910
-120.00	0.0004619	0.0920	0.284	5.090
-100.00	0.0004744	0.0950	0.284	5.280
-80.00	0.0004814	0.0980	0.284	5.430
-60.00	0.0004883	0.1000	0.284	5.580
-40.00	0.0004953	0.1020	0.284	5.720
-20.00	0.0005022	0.1040	0.284	5.860
0.00	0.0005092	0.1055	0.284	6.000
20.00	0.0005125	0.1070	0.284	6.120
40.00	0.0005158	0.1080	0.284	6.240
60.00	0.0005194	0.1090	0.284	6.360
80.00	0.0005231	0.1100	0.284	6.470

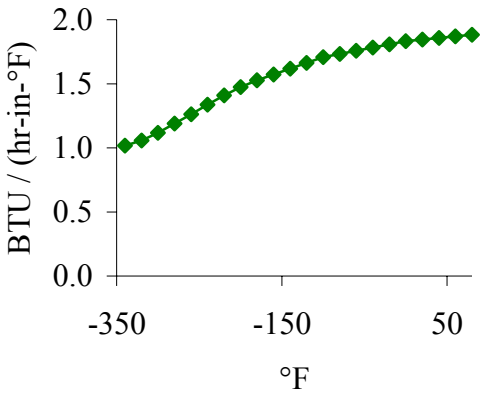

Figure A5. Thermal Conductivity of ASTM A203-A Steel as a Function of Temperature

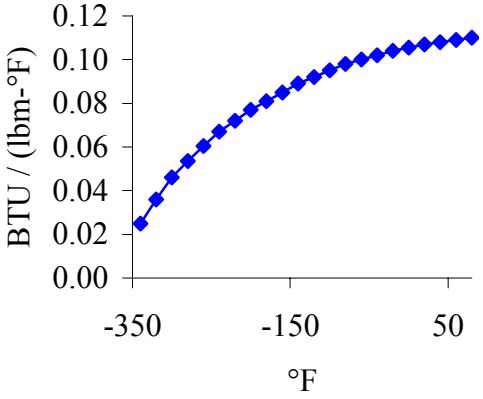

Figure A6. Specific Heat of ASTM A203-A Steel as a Function of Temperature

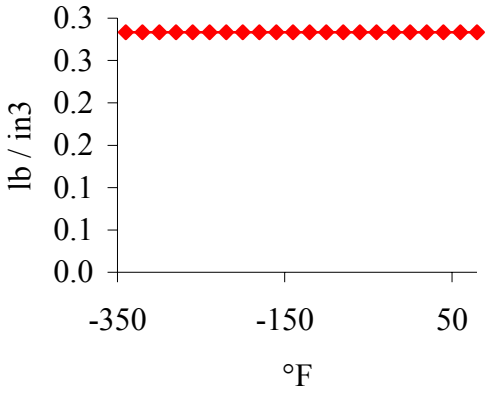

Figure A7. Density of ASTM A203-A Steel as a Function of Temperature

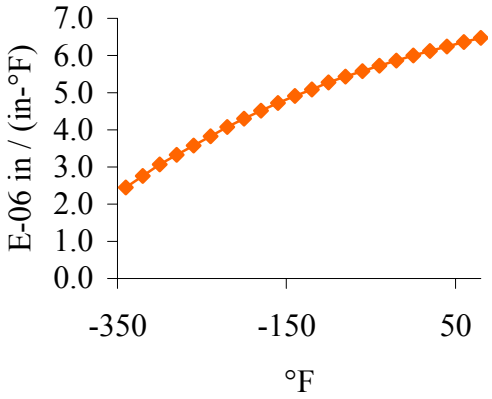

Figure A8. Coefficient of Thermal Expansion of ASTM A203-A Steel as a Function of Temperature

The fracture toughness is also an important parameter in this study. No exact data was found for this quantity. The data was extracted from the following graph:

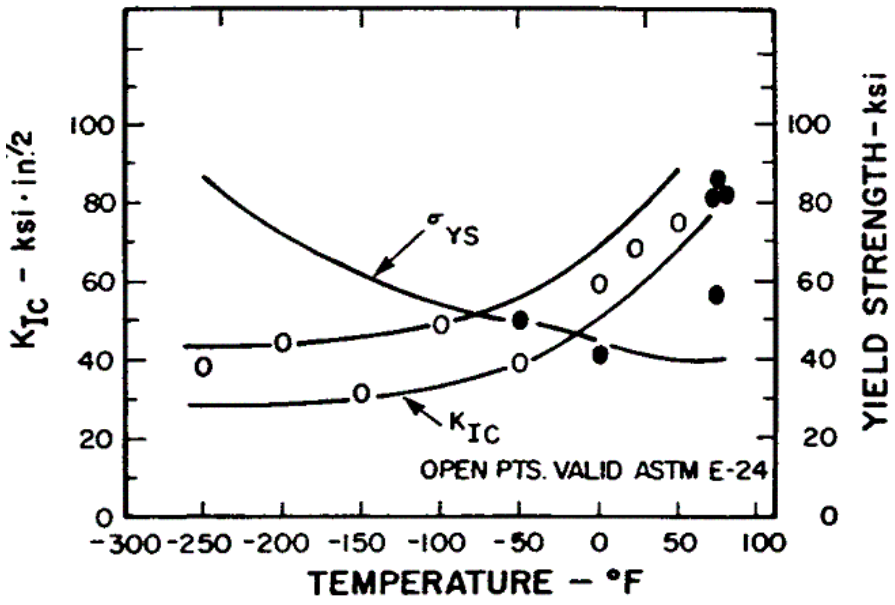

Figure A9. Fracture Toughness and Yield Strength as a Function of Temperature (Source: Greenberg, 1969)

Discrete points were approximated by using the lower fracture toughness curve. These points are listed in Table A3. Although this is the fracture Toughness of ASTM E-24 Steel, it is a representative number of all steels.

Table A3. Fracture Toughness of ASTM E-24 Steel as a Function of Temperature

Temperature	Fracture Toughness
°F	$ksi\sqrt{in}$
-250.0	28
-200.0	29
-150.0	30
-100.0	34
-50.0	39
0.0	51
50.0	68
70.0	77

Appendix 2: Convection Medium Property Data

The heat transfer coefficients for convection into liquid nitrogen are not constants. The following graph was used to get these coefficients.

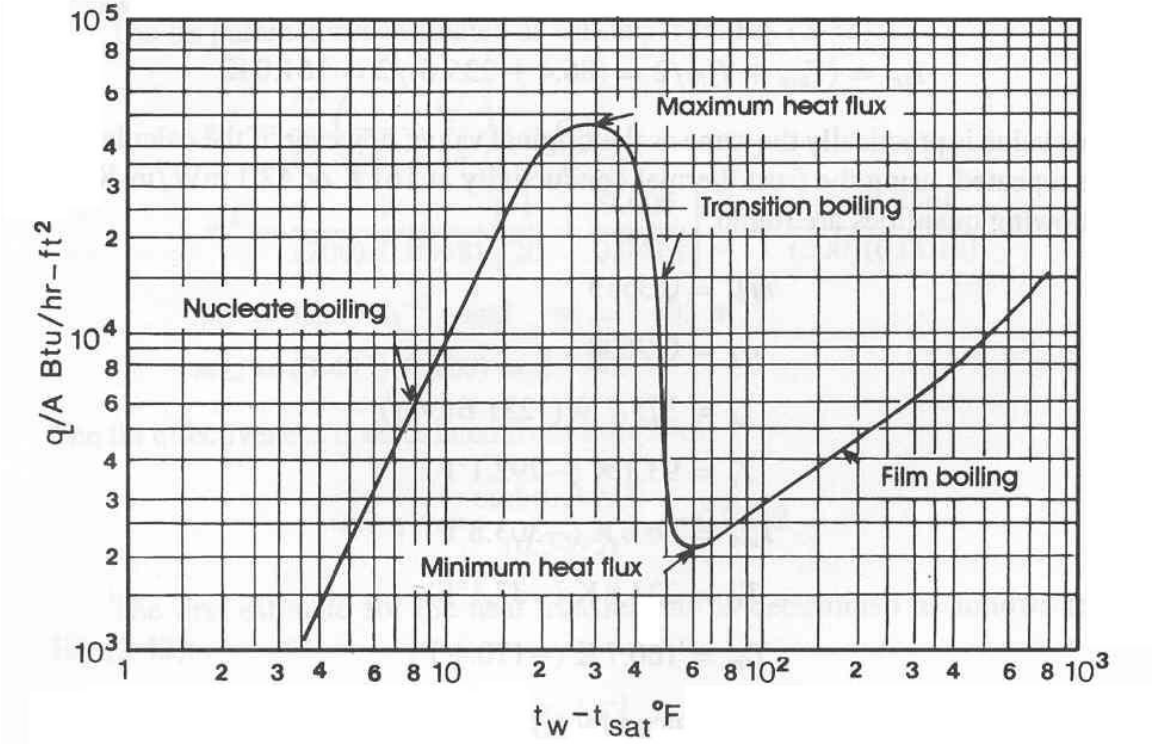

Figure A10. Heat Flux Versus Temperature Difference for Liquid Nitrogen (Source: Barron, 1999)

The curve is a plot of the amount of heat flux versus the temperature difference between the wall and the fluid. The convection coefficient is found by taking points from this graph and dividing the heat flux at a point by the temperature difference at the wall. This yields a table of values which are presented below.

Table A4. Convection Coefficient for Liquid Nitrogen as a Function of Temperature

Wall Temperature	Coefficient	Wall Temperature	Coefficient
°F	BTU / (in^2-sec)	°F	BTU / (in^2-sec)
-320	0.000579	-240	5.88E-05
-318	0.000579	-230	5.67E-05
-316	0.000849	-220	5.59E-05
-314	0.001213	-210	5.47E-05
-312	0.001586	-200	5.31E-05
-310	0.002067	-190	5.15E-05
-308	0.00256	-180	5.00E-05
-306	0.003022	-170	4.88E-05
-304	0.003426	-160	4.78E-05
-302	0.003696	-150	4.71E-05
-300	0.003776	-140	4.65E-05
-298	0.003697	-130	4.59E-05
-296	0.003549	-120	4.53E-05
-294	0.003384	-110	4.46E-05
-292	0.003195	-100	4.38E-05
-290	0.002967	-90	4.30E-05
-288	0.002704	-80	4.23E-05
-286	0.002425	-70	4.16E-05
-284	0.002136	-60	4.10E-05
-282	0.001818	-50	4.04E-05
-280	0.001448	-40	3.99E-05
-278	0.001047	-30	3.95E-05
-276	0.00067	-20	3.92E-05
-274	0.000362	-10	3.90E-05
-272	0.000161	0	3.88E-05
-270	9.46E-05	10	3.87E-05
-268	8.20E-05	20	3.86E-05
-266	7.72E-05	30	3.86E-05
-264	7.38E-05	40	3.86E-05
-262	7.11E-05	50	3.86E-05
-260	6.93E-05	60	3.86E-05
-250	6.28E-05	70	3.86E-05
		80	3.86E-05

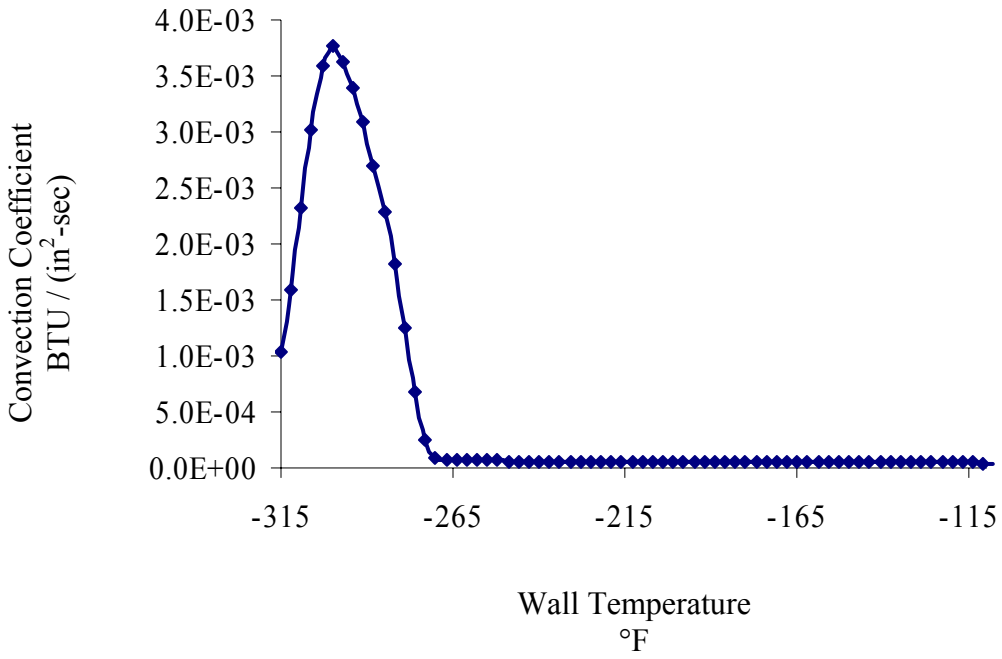

Figure A11. Convection Coefficient for Liquid Nitrogen as a Function of Wall Temperature

The convection coefficients for the other media were calculated within the program at run-time. This is based on the following method. First property data must be obtained for air and alcohol.

Table A5. Property Data for Air as a Function of Temperature

Refrigerated air was assumed to be at -30 °F.				
Temperature	Volumetric Expansion	Kinematic Viscosity	Thermal Diffusivity	Thermal Conductivity
°F	1/R	in^2/sec	in^2/sec	BTU / (sec-ft-°F)
-238	4.56E-03	4.82E-11	6.49E-11	1.61E-07
-148	3.23E-03	9.24E-11	1.28E-10	2.21E-07
-58	2.51E-03	1.48E-10	2.08E-10	2.76E-07
32	2.04E-03	2.06E-10	2.90E-10	3.24E-07
68	1.91E-03	2.34E-10	3.32E-10	3.44E-07
104	1.78E-03	2.63E-10	3.70E-10	3.62E-07
140	1.67E-03	2.93E-10	4.14E-10	3.81E-07
176	1.57E-03	3.25E-10	4.59E-10	4.00E-07
212	1.49E-03	3.57E-10	5.08E-10	4.20E-07
248	1.42E-03	3.91E-10	5.60E-10	4.39E-07
284	1.35E-03	4.27E-10	6.15E-10	4.59E-07
320	1.29E-03	4.63E-10	6.67E-10	4.79E-07
356	1.23E-03	5.00E-10	7.24E-10	4.98E-07
392	1.17E-03	5.37E-10	7.83E-10	5.16E-07
482	1.06E-03	6.38E-10	9.35E-10	5.63E-07
572	9.72E-04	7.42E-10	1.09E-09	5.22E-07
662	8.94E-04	8.53E-10	1.26E-09	6.49E-07
752	8.28E-04	9.69E-10	1.42E-09	6.90E-07

The alcohol used in the dry-ice/alcohol mixture is isopropyl. These properties were found using AspenPlus (AspenTech, 2004).

Table A6. Property Data for Isopropyl Alcohol as a Function of Temperature

The alcohol was assumed to be at -108 °F				
Temperature	Volumetric Expansion	Kinematic Viscosity	Thermal Diffusivity	Thermal Conductivity
°F	1/R	in^2/sec	in^2/sec	BTU / (sec-ft-°F)
-100	4.50E-04	2.27E-01	1.23E-04	2.11E-06
-90	4.50E-04	1.63E-01	1.21E-04	2.09E-06
-80	4.50E-04	1.19E-01	1.19E-04	2.07E-06
-70	4.50E-04	8.87E-02	1.17E-04	2.05E-06
-60	4.50E-04	6.69E-02	1.16E-04	2.04E-06
-50	4.50E-04	5.12E-02	1.14E-04	2.02E-06
-40	4.50E-04	3.96E-02	1.12E-04	2.00E-06
-30	4.50E-04	3.10E-02	1.10E-04	1.99E-06
-20	4.50E-04	2.46E-02	1.08E-04	1.97E-06
-10	4.50E-04	1.97E-02	1.06E-04	1.95E-06
0	4.50E-04	1.59E-02	1.04E-04	1.94E-06

From this data, and the specific wall temperature and cylinder diameter, the Grashof, Prandtl, and Raleigh number were calculated using the following formulas. (Incropera, 1996)

$$\mathrm{Gr} = \frac{g\beta(T_{wall} - T_{fluid})D^3}{\upsilon_k{}^2} \tag{88}$$

$$\mathrm{Pr} = \frac{\upsilon_k}{\alpha} \tag{89}$$

$$\mathrm{Ra} = \mathrm{Gr} \cdot \mathrm{Pr} \tag{90}$$

where,

g is the gravitational constant,

β is the volumetric thermal expansion coefficient,

T_{wall} is the temperature of the wall,

T_{fluid} is the temperature of the fluid,

D is the diameter of the surface from convection is taking place,

υ_k is the kinematic viscosity of the fluid,

Gr is the Grashof number,

Pr is the Prandtl number, and

Ra is the Raleigh number.

From these quantities, the Nusselt number was calculated. A correlation for a vertical cylinder was not found. The correlation for a vertical plate functions similarly and thus the following Nusselt number was calculated from which the convection coefficient is estimated.

$$Nu = \left(0.825 + \frac{0.387 Ra^{\frac{1}{6}}}{\left(1 + \left(\frac{0.492}{\mathrm{Pr}} \right)^{\frac{9}{16}} \right)^{\frac{8}{27}}} \right)^2 \tag{91}$$

$$h = \frac{Nu \cdot k}{D} \tag{92}$$

where,

Nu is the Nusselt number,

h is the convection coefficient,

and k is the thermal conductivity of the fluid.

This process was done to approximate the convection coefficient for refrigerated air and dry-ice/alcohol.

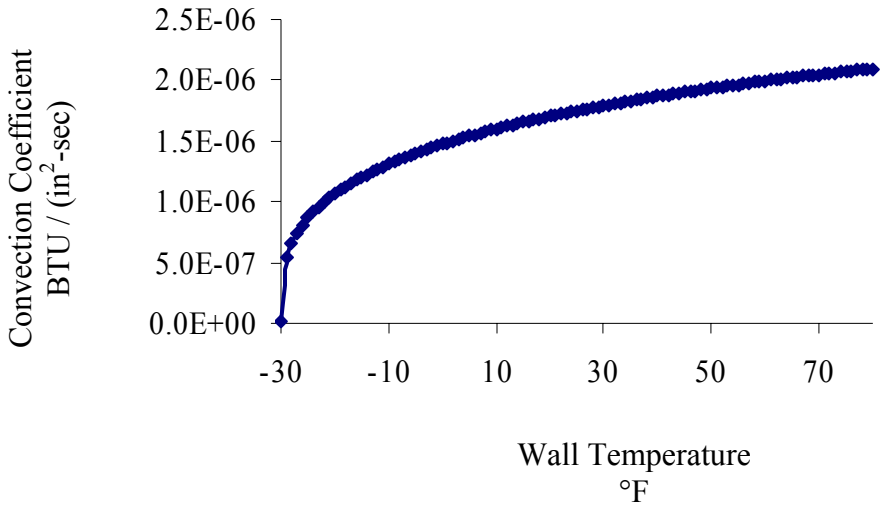

Figure A12. Convection Coefficient for Air as a Function of Wall Temperature for a Diameter = 1 in

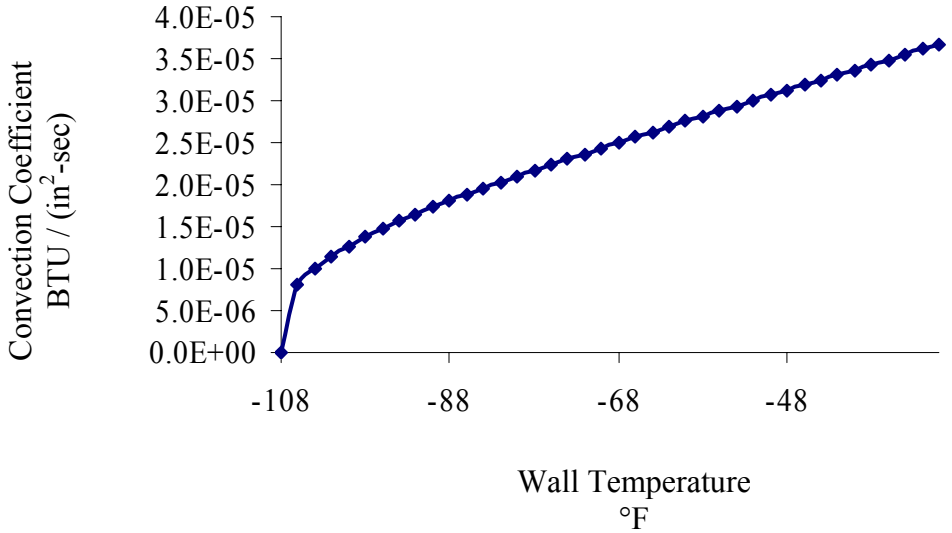

Figure A13. Convection Coefficient for Dry-Ice/Alcohol as a Function of Wall Temperature for a Diameter = 1 in

Appendix 3: Program Flow

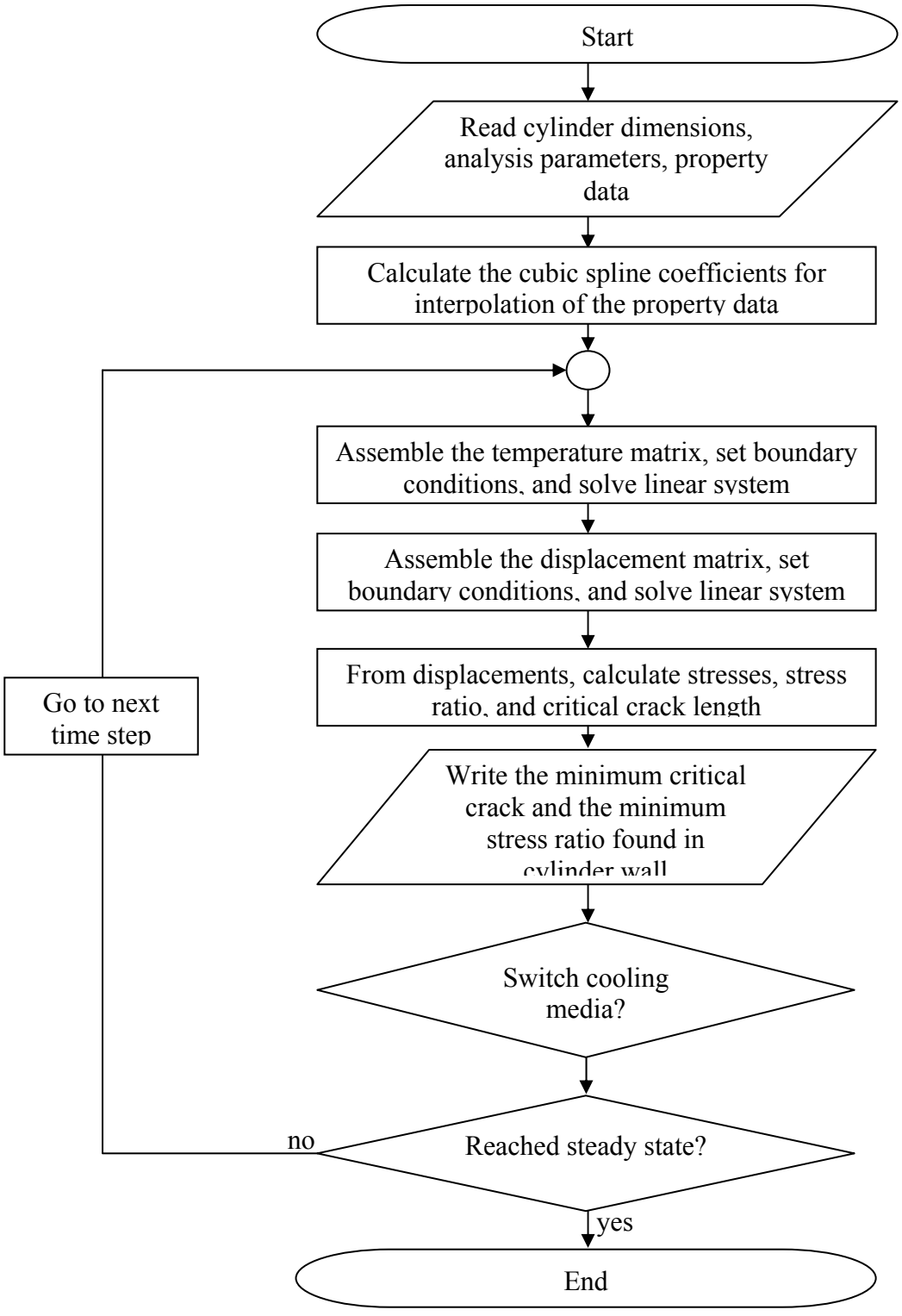

Figure A14. Flow Chart of Computer Program

Appendix 4: Verification

Several tests were run to ensure the program written was correct for simpler cases. Although this does not prove that the more complex cases will be correct, it does suggest that the approximations were handled correctly.

First the temperature portion was verified. A problem was taken out of a text book for heat transfer where the diameter was very small and thus the temperature distribution virtually constant. The temperature as a function of time is desired in this case. There are two cases involving placing the cylinder in water and also in air. Both cases were run. The problem comes from (Kreith, 1986). Being an example problem, the solution is worked out and plotted. Due to the fact that the problem involves a solid cylinder, it was necessary to change the program. This is actually only involved changing one number, the one indicating the flux at the center. Below is the plot of the exact solution and the program.

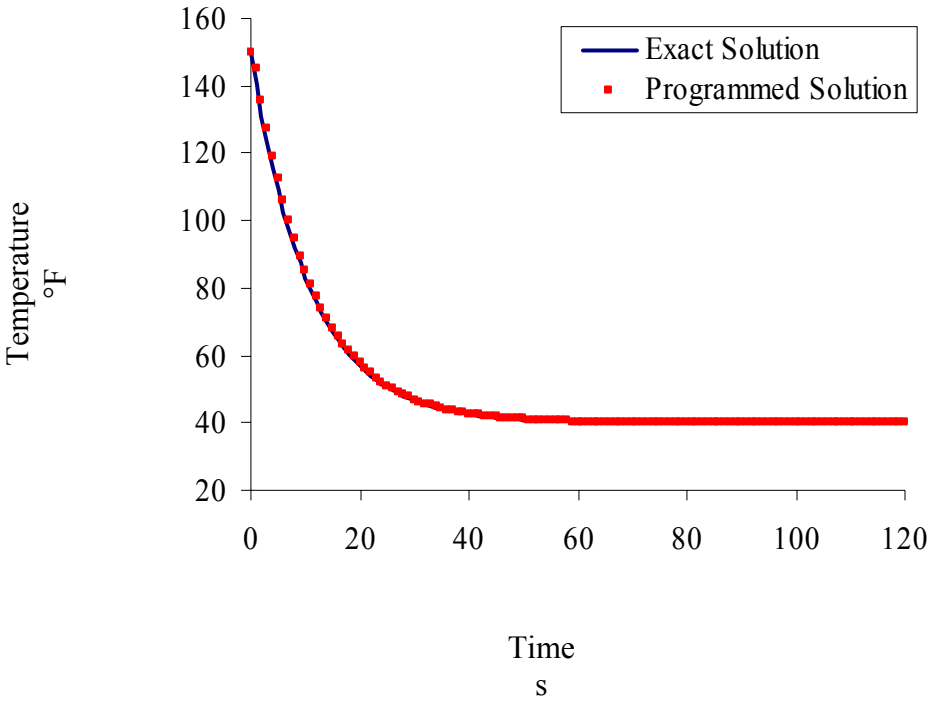

Figure A15. Comparison of Exact and Programmed Solution to the Water Problem

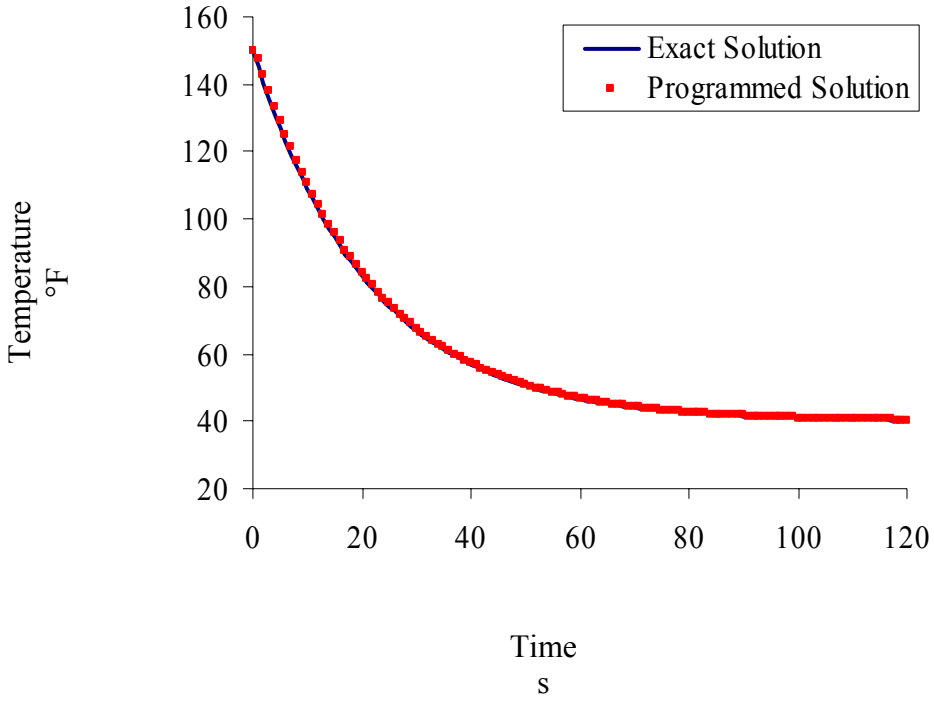

Figure A16. Comparison of Exact and Programmed Solution to the Air Problem

The maximum true error from Figs. A13 and A14 is 4%. This suggests that the thermal portion is approximating correctly.

The stresses were also verified. Initially, the elasticity part was written separated form the thermal part. A function was used to input a temperature matrix as if it were the steady state temperature distribution. This allowed for checking in multiple ways. If the material properties are made constant, and a temperature distribution specified, the stresses can be written explicitly.

Appendix 5: Convergence Test

Two convergence tests were run to determine how many radial divisions and time divisions were necessary to obtain good results. This test also confirms that the solution is converging. A node near the inner surface was chosen for study. The temperature at that node was recorded using three increasingly fine radial meshes. This is a good choice of node because the temperature gradient is high there. This will be the greatest chance to study how the displacement changes as the number of radial divisions increase. The following details the method for such a test and gives the results for this analysis.

The temperature, R_N, at a point (Logan, 1992) is given by:

$$R_N = A + \frac{B}{(N)^{\alpha}} \tag{93}$$

where

B and α = constants,

A = extrapolated result for infinite mesh density, and

N = number of elements.

Note that if α is greater that one, as N becomes larger (infinite) the temperature becomes equal to a value A. For the solution to converge, it is necessary that $\alpha > 1$. The solution will converge on the value of A. Three temperatures were calculated using three different radial divisions. This generates a system of equations for which A, B, and α are solved.

$$R_{16} = 69.1895 = A + \frac{B}{16^{\alpha}} \tag{94}$$

$$R_{32} = 73.2526 = A + \frac{B}{32^{\alpha}} \tag{95}$$

$$R_{64} = 74.6831 = A + \frac{B}{64^{\alpha}} \tag{96}$$

Simultaneously solving these three equations for A, B and α yields A=75.4605 in, B=-408.0736, and α=1.5060. Since α>1, the results will converge. If 64 radial divisions are used, the answer obtained is 1% different from the value of A. This indicates that 64 radial divisions are sufficient for good results. This is valid for the cylinder dimensions used in this experiment. As stated in the results section, in this analysis the outer diameter

of the hub is to be varied. In other cases, 64 radial divisions may not be ample to ensure good results. Therefore a proportional amount of radial divisions were used so that the distance between radial divisions would remain the same.

The same test was run for the number of time divisions. As in the previous experiment, the same node was chosen and studied using 64 radial divisions, this time changing the time step between iterations. The following are those results.

$$R_2 = 74.6831 = A + \frac{B}{2^{\alpha}} \tag{97}$$

$$R_4 = 74.1777 = A + \frac{B}{4^{\alpha}} \tag{98}$$

$$R_8 = 73.9309 = A + \frac{B}{8^{\alpha}} \tag{99}$$

Simultaneously solving these three equations for A, B and α yields A=73.6955 in, B=2.02286, and α =1.0345. Again, the solution is converging. Using 8 time divisions, the answer obtained is <1% different from the value of A. This indicates that the answer has indeed converged. Therefore 8 time divisions were used which corresponds to a time step of 0.5 seconds.

Appendix 6: Tables of Results

Table A7. Results for the Christa McAuliffe in Cooling Process 1

Outer Radius of Cylinder 2	Interference	Critical Crack Length	Location of Critical Crack	Minimum Stress Ratio	Location of Minimum Stress Ratio
in	in	in	in	non-dim	in
10.800	4.74E-03	0.173	10.800	4.779	1.000
11.736	4.74E-03	0.182	11.736	3.965	1.000
12.672	4.74E-03	0.186	12.672	3.464	1.000
13.608	4.74E-03	0.187	13.608	3.123	1.000
14.544	4.74E-03	0.186	14.544	2.872	1.000
15.480	4.74E-03	0.182	15.480	2.678	1.000
16.416	4.74E-03	0.177	16.416	2.521	1.000
17.352	4.74E-03	0.172	17.352	2.390	1.000
18.288	4.74E-03	0.165	18.288	2.277	1.000
19.224	4.74E-03	0.159	19.224	2.178	1.000
10.800	8.62E-03	0.101	10.800	3.511	1.000
11.736	8.62E-03	0.113	11.736	2.759	1.000
12.672	8.62E-03	0.122	12.672	2.333	1.000
13.608	8.62E-03	0.130	13.608	2.072	1.000
14.544	8.62E-03	0.134	14.544	1.896	1.000
15.480	8.62E-03	0.137	15.480	1.769	1.000
16.416	8.62E-03	0.138	16.416	1.674	1.000
17.352	8.62E-03	0.137	17.352	1.599	1.000
18.288	8.62E-03	0.135	18.288	1.539	1.000
19.224	8.62E-03	0.133	19.224	1.487	1.000

Table A8. Results for the Christa McAuliffe in Cooling Process 2

Outer Radius of Cylinder 2	Interference	Critical Crack Length	Location of Critical Crack	Minimum Stress Ratio	Location of Minimum Stress Ratio
in	in	in	in	non-dim	in
10.8000	4.74E-03	0.3879	10.8000	6.8616	1.0000
11.7360	4.74E-03	0.4436	11.7360	5.3135	1.0000
12.6720	4.74E-03	0.4905	12.6720	4.4956	1.0000
13.6080	4.74E-03	0.5276	13.6080	3.9903	1.0000
14.5440	4.74E-03	0.5523	14.5440	3.6467	1.0000
15.4800	4.74E-03	0.5589	15.4800	3.3975	1.0000
16.4160	4.74E-03	0.5597	16.4160	3.2085	1.0000
17.3520	4.74E-03	0.5562	17.3520	3.0601	1.0000
18.2880	4.74E-03	0.5494	18.2880	2.9407	1.0000
19.2240	4.74E-03	0.5402	19.2240	2.8426	1.0000
10.8000	8.62E-03	0.1800	10.8000	4.3065	1.0000
11.7360	8.62E-03	0.2190	11.7360	3.2831	1.0000
12.6720	8.62E-03	0.2571	12.6720	2.7607	1.0000
13.6080	8.62E-03	0.2926	13.6080	2.4449	1.0000
14.5440	8.62E-03	0.3245	14.5440	2.2337	1.0000
15.4800	8.62E-03	0.3520	15.4800	2.0830	1.0000
16.4160	8.62E-03	0.3746	16.4160	1.9702	1.0000
17.3520	8.62E-03	0.3917	17.3520	1.8829	1.0000
18.2880	8.62E-03	0.4000	18.2880	1.8133	1.0000
19.2240	8.62E-03	0.4052	19.2240	1.7568	1.0000

Table A9. Results for the Christa McAuliffe in Cooling Process 3

Outer Radius of Cylinder 2	Interference	Critical Crack Length	Location of Critical Crack	Minimum Stress Ratio	Location of Minimum Stress Ratio
in	in	in	in	non-dim	in
10.8000	4.74E-03	0.3880	10.8000	8.4047	1.0000
11.7360	4.74E-03	0.4440	11.7360	6.4427	1.0000
12.6720	4.74E-03	0.4912	12.6720	5.3498	1.0000
13.6080	4.74E-03	0.5288	13.6080	4.7070	1.0000
14.5440	4.74E-03	0.5568	14.5440	4.2855	1.0000
15.4800	4.74E-03	0.5758	15.4800	3.9889	1.0000
16.4160	4.74E-03	0.5870	16.4160	3.7696	1.0000
17.3520	4.74E-03	0.5916	17.3520	3.6012	1.0000
18.2880	4.74E-03	0.5908	18.2880	3.4682	1.0000
19.2240	4.74E-03	0.5859	19.2240	3.3606	1.0000
10.8000	8.62E-03	0.1801	10.8000	4.7867	1.0000
11.7360	8.62E-03	0.2191	11.7360	3.5551	1.0000
12.6720	8.62E-03	0.2573	12.6720	2.9577	1.0000
13.6080	8.62E-03	0.2931	13.6080	2.6075	1.0000
14.5440	8.62E-03	0.3254	14.5440	2.3786	1.0000
15.4800	8.62E-03	0.3535	15.4800	2.2183	1.0000
16.4160	8.62E-03	0.3769	16.4160	2.1003	1.0000
17.3520	8.62E-03	0.3957	17.3520	2.0102	1.0000
18.2880	8.62E-03	0.4101	18.2880	1.9395	1.0000
19.2240	8.62E-03	0.4204	19.2240	1.8820	1.0000

Table A10. Results for Hillsborough Ave. in Cooling Process 1

Outer Radius of Cylinder 2	Interference	Critical Crack Length	Location of Critical Crack	Minimum Stress Ratio	Location of Minimum Stress Ratio
in	in	in	in	non-dim	in
10.068	4.63E-03	0.178	10.068	5.100	1.125
10.941	4.63E-03	0.190	10.941	4.193	1.125
11.813	4.63E-03	0.196	11.813	3.642	1.125
12.686	4.63E-03	0.199	12.686	3.271	1.125
13.558	4.63E-03	0.199	13.558	3.004	1.125
14.431	4.63E-03	0.197	14.431	2.801	1.125
15.303	4.63E-03	0.192	15.303	2.639	1.125
16.176	4.63E-03	0.187	16.176	2.505	1.125
17.048	4.63E-03	0.181	17.048	2.393	1.125
17.921	4.63E-03	0.174	17.921	2.295	1.125
10.068	8.42E-03	0.101	10.068	3.653	1.125
10.941	8.42E-03	0.114	10.941	2.856	1.125
11.813	8.42E-03	0.126	11.813	2.393	1.125
12.686	8.42E-03	0.134	12.686	2.114	1.125
13.558	8.42E-03	0.140	13.558	1.928	1.125
14.431	8.42E-03	0.144	14.431	1.795	1.125
15.303	8.42E-03	0.146	15.303	1.696	1.125
16.176	8.42E-03	0.146	16.176	1.619	1.125
17.048	8.42E-03	0.146	17.048	1.558	1.125
17.921	8.42E-03	0.144	17.921	1.507	1.125

Table A11. Results for Hillsborough Ave. in Cooling Process 2

Outer Radius of Cylinder 2	Interference	Critical Crack Length	Location of Critical Crack	Minimum Stress Ratio	Location of Minimum Stress Ratio
in	in	in	in	non-dim	in
10.0680	4.63E-03	0.3846	10.0680	7.3378	1.1250
10.9406	4.63E-03	0.4454	10.9406	5.5702	1.1250
11.8131	4.63E-03	0.4983	11.8131	4.6679	1.1250
12.6857	4.63E-03	0.5419	12.6857	4.1214	1.1250
13.5582	4.63E-03	0.5757	13.5582	3.7549	1.1250
14.4308	4.63E-03	0.5951	14.4308	3.4919	1.1250
15.3034	4.63E-03	0.5984	15.3034	3.2937	1.1250
16.1759	4.63E-03	0.5967	16.1759	3.1386	1.1250
17.0485	4.63E-03	0.5911	17.0485	3.0140	1.1250
17.9210	4.63E-03	0.5825	17.9210	2.9118	1.1250
10.0680	8.42E-03	0.1739	10.0680	4.4071	1.1250
10.9406	8.42E-03	0.2138	10.9406	3.3173	1.1250
11.8131	8.42E-03	0.2537	11.8131	2.7731	1.1250
12.6857	8.42E-03	0.2918	12.6857	2.4483	1.1250
13.5582	8.42E-03	0.3269	13.5582	2.2331	1.1250
14.4308	8.42E-03	0.3576	8.3900	2.0807	1.1250
15.3034	8.42E-03	0.3800	8.3900	1.9673	1.1250
16.1759	8.42E-03	0.4004	8.3900	1.8799	1.1250
17.0485	8.42E-03	0.4190	8.3900	1.8105	1.1250
17.9210	8.42E-03	0.4279	17.9210	1.7540	1.1250

Table A12. Results for Hillsborough Ave. in Cooling Process 3

Outer Radius of Cylinder 2	Interference	Critical Crack Length	Location of Critical Crack	Minimum Stress Ratio	Location of Minimum Stress Ratio
in	in	in	in	non-dim	in
10.0680	4.63E-03	0.3847	10.0680	8.2885	1.1250
10.9406	4.63E-03	0.4456	10.9406	6.1590	1.1250
11.8131	4.63E-03	0.4987	11.8131	5.1261	1.1250
12.6857	4.63E-03	0.5427	12.6857	4.5204	1.1250
13.5582	4.63E-03	0.5770	13.5582	4.1246	1.1250
14.4308	4.63E-03	0.6020	14.4308	3.8474	1.1250
15.3034	4.63E-03	0.6185	15.3034	3.6433	1.1250
16.1759	4.63E-03	0.6276	16.1759	3.4862	1.1250
17.0485	4.63E-03	0.6304	17.0485	3.3579	1.1250
17.9210	4.63E-03	0.6283	17.9210	3.2543	1.1250
10.0680	8.42E-03	0.1739	10.0680	4.5627	1.1250
10.9406	8.42E-03	0.2139	10.9406	3.3909	1.1250
11.8131	8.42E-03	0.2538	11.8131	2.8224	1.1250
12.6857	8.42E-03	0.2921	12.6857	2.4891	1.1250
13.5582	8.42E-03	0.3275	13.5582	2.2713	1.1250
14.4308	8.42E-03	0.3576	8.3900	2.1188	1.1250
15.3034	8.42E-03	0.3800	8.3900	2.0066	1.1250
16.1759	8.42E-03	0.4004	8.3900	1.9209	1.1250
17.0485	8.42E-03	0.4190	8.3900	1.8536	1.1250
17.9210	8.42E-03	0.4360	8.3900	1.7996	1.1250

Table A13. Results for 17th St. Causeway in Cooling Process 1

Outer Radius of Cylinder 2	Interference	Critical Crack Length	Location of Critical Crack	Minimum Stress Ratio	Location of Minimum Stress Ratio
in	in	in	in	non-dim	in
7.766	4.25E-03	0.184	7.766	5.298	1.188
8.439	4.25E-03	0.204	8.439	4.303	1.188
9.113	4.25E-03	0.219	9.113	3.717	1.188
9.786	4.25E-03	0.230	9.786	3.326	1.188
10.459	4.25E-03	0.236	10.459	3.019	1.188
11.132	4.25E-03	0.240	11.132	2.790	1.188
11.805	4.25E-03	0.240	11.805	2.619	1.188
12.478	4.25E-03	0.238	12.478	2.486	1.188
13.151	4.25E-03	0.235	13.151	2.381	1.188
13.824	4.25E-03	0.230	13.824	2.295	1.188
7.766	7.72E-03	0.094	7.766	3.602	1.188
8.439	7.72E-03	0.111	8.439	2.686	1.188
9.113	7.72E-03	0.127	9.113	2.224	1.188
9.786	7.72E-03	0.141	9.786	1.951	1.188
10.459	7.72E-03	0.153	10.459	1.771	1.188
11.132	7.72E-03	0.162	11.132	1.644	1.188
11.805	7.72E-03	0.169	11.805	1.549	1.188
12.478	7.72E-03	0.174	12.478	1.477	1.188
13.151	7.72E-03	0.177	13.151	1.419	1.188
13.824	7.72E-03	0.178	13.824	1.372	1.188

Table A14. Results for 17th St. Causeway in Cooling Process 2

Outer Radius of Cylinder 2	Interference	Critical Crack Length	Location of Critical Crack	Minimum Stress Ratio	Location of Minimum Stress Ratio
in	in	in	in	non-dim	in
7.7664	4.25E-03	0.3491	7.7664	6.8990	1.1875
8.4395	4.25E-03	0.4206	8.4395	5.1363	1.1875
9.1126	4.25E-03	0.4890	9.1126	4.2811	1.1875
9.7857	4.25E-03	0.5517	9.7857	3.7795	1.1875
10.4588	4.25E-03	0.6070	10.4588	3.4516	1.1875
11.1318	4.25E-03	0.6537	11.1318	3.2178	1.1875
11.8049	4.25E-03	0.6916	11.8049	3.0329	1.1875
12.4780	4.25E-03	0.7206	12.4780	2.8902	1.1875
13.1511	4.25E-03	0.7414	13.1511	2.7769	1.1875
13.8242	4.25E-03	0.7398	13.8242	2.6846	1.1875
7.7664	7.72E-03	0.1403	6.4720	3.7989	1.1875
8.4395	7.72E-03	0.1694	6.4720	2.8284	1.1875
9.1126	7.72E-03	0.1978	6.4720	2.3575	1.1875
9.7857	7.72E-03	0.2213	6.4720	2.0814	1.1875
10.4588	7.72E-03	0.2408	6.4720	1.9009	1.1875
11.1318	7.72E-03	0.2587	6.4720	1.7746	1.1875
11.8049	7.72E-03	0.2751	6.4720	1.6816	1.1875
12.4780	7.72E-03	0.2900	6.4720	1.6107	1.1875
13.1511	7.72E-03	0.3037	6.4720	1.5550	1.1875
13.8242	7.72E-03	0.3161	6.4720	1.5102	1.1875

Table A15. Results for 17th St. Causeway in Cooling Process 3

Outer Radius of Cylinder 2	Interference	Critical Crack Length	Location of Critical Crack	Minimum Stress Ratio	Location of Minimum Stress Ratio
in	in	in	in	non-dim	in
7.7664	4.25E-03	0.3491	7.7664	6.9086	1.1875
8.4395	4.25E-03	0.4206	8.4395	5.1422	1.1875
9.1126	4.25E-03	0.4890	9.1126	4.2856	1.1875
9.7857	4.25E-03	0.5518	9.7857	3.7834	1.1875
10.4588	4.25E-03	0.6072	10.4588	3.4552	1.1875
11.1318	4.25E-03	0.6541	11.1318	3.2254	1.1875
11.8049	4.25E-03	0.6922	11.8049	3.0563	1.1875
12.4780	4.25E-03	0.7216	12.4780	2.9273	1.1875
13.1511	4.25E-03	0.7428	13.1511	2.8259	1.1875
13.8242	4.25E-03	0.7567	13.8242	2.7446	1.1875
7.7664	7.72E-03	0.1403	6.4720	3.8018	1.1875
8.4395	7.72E-03	0.1694	6.4720	2.8302	1.1875
9.1126	7.72E-03	0.1978	6.4720	2.3589	1.1875
9.7857	7.72E-03	0.2213	6.4720	2.0826	1.1875
10.4588	7.72E-03	0.2408	6.4720	1.9020	1.1875
11.1318	7.72E-03	0.2587	6.4720	1.7756	1.1875
11.8049	7.72E-03	0.2751	6.4720	1.6826	1.1875
12.4780	7.72E-03	0.2900	6.4720	1.6116	1.1875
13.1511	7.72E-03	0.3037	6.4720	1.5559	1.1875
13.8242	7.72E-03	0.3161	6.4720	1.5112	1.1875